nature cell biology

Live-imaging of single stem cells within their niche reveals that a U3snoRNP component segregates asymmetrically and is required for self-renewal in *Drosophila*

Pierre Fichelson[1,4,6], Clara Moch[1,3,6], Kenzo Ivanovitch[1,4], Charlotte Martin[2,3], Clara M Sidor[1,5], Jean-Antoine Lepesant[1], Yohanns Bellaiche[2,3] and Jean-René Huynh[1,3,7]

Stem cells generate self-renewing and differentiating progeny over many rounds of asymmetric divisions. How stem cell growth rate and size are maintained over time remains unknown. We isolated mutations in a *Drosophila melanogaster* gene, *wicked* (*wcd*), which induce premature differentiation of germline stem cells (GSCs). Wcd is a member of the U3 snoRNP complex required for pre-ribosomal RNA maturation. This general function of Wcd contrasts with its specific requirement for GSC self-renewal. However, live imaging of GSCs within their niche revealed a pool of Wcd-forming particles that segregate asymmetrically into the GSCs on mitosis, independently of the Dpp signal sent by the niche. A fraction of Wcd also segregated asymmetrically in dividing larval neural stem cells (NSCs). In the absence of Wcd, NSCs became smaller and produced fewer neurons. Our results show that regulation of ribosome synthesis is a crucial parameter for stem cell maintenance and function.

During development or after injury, stem cells face the dual task of generating tissue and maintaining their own cell population with identical properties for tissue homeostasis[1]. One of these properties is stem cell size, which is restored rapidly after division. How stem cell growth is regulated and whether this regulation is required for their function is poorly characterized.

Drosophila GSCs are a good model to study actively proliferating stem cells, as they produce gametes throughout adult life[2]. In females, GSCs are located at the apex of a structure called the germarium[3,4] (Fig. 1a). Two to three GSCs adhere to a niche of somatic cells, providing signals that prevent GSC differentiation, such as Decapentaplegic (Dpp, a bone morphogenetic protein)[5,6]. GSCs divide asymmetrically, generating daughter cells with distinct fates[7]. Upon division, the orientation of the mitotic spindle allows at least one daughter to remain within the niche and adopt the GSC fate, while its sibling positioned outside the niche differentiates into a cystoblast[8,9]. The cytoblast undergoes four rounds of asymmetric divisions with incomplete cytokinesis, producing a cyst of 16 cells (cystocytes) interconnected by cytoplasmic bridges called ring canals[10,11]. The asymmetry of the GSC division relies mainly on extrinsic mechanisms[3,4]. The only known intrinsic asymmetry of female GSC division is the differential segregation of the spectrosome, a cytoplasmic structure made of vesicles kept together by components of the submembraneous cytoskeleton[8,12]. During the four cyst divisions, a spectrosome-like structure, the fusome, anchors one pole of each spindle and ensures that an invariant pattern of divisions is followed[13]. This pattern is important as the oocyte differentiates from one of the two cells with four ring canals, which are called pro-oocytes. Cystocyte size decreases after each division, whereas GSC size is maintained over time and many divisions[14]. How GSC growth is regulated remains unknown.

Cell growth depends primarily on ribosome biogenesis, as the amount of ribosomes in a cell determines the quantity of proteins that can be synthesised[15–17]. Ribosome biogenesis begins with transcription of the ribosomal genes, and maturation of the 47S pre-ribosomal RNA (pre-rRNA) in the nucleolus[18]. The pre-rRNA matures through methylations and pseudouridylations together with endonucleolytic and exonucleolytic cleavages of external and internal transcribed spacers (ETS and ITS). These maturation steps are carried out by complexes containing small nucleolar RNAs (snoRNAs) together with associated proteins called small nucleolar ribonucleoproteins (snoRNPs)[19]. The release of 18S rRNA from the pre-rRNA requires U3 snoRNA, which is associated with pre-rRNA processing components such as Fibrillarin (Fib). Once cleaved, the matured rRNAs assemble with ribosomal proteins and form the 60S and 40S ribosome subunits. Although ribosome biogenesis has been well

[1]Institut Jacques Monod, CNRS, Universités Paris 6 et 7, 2, place Jussieu, F-75251 Paris, Cedex 05, France. [2]Institut Curie, UMR 144, 26 rue d'Ulm, 75248 Paris, Cedex 05, France. Current addresses: [3]Institute Curie, Department of Genetics and Developmental Biology (U934/UMR3215), 26 rue d'Ulm, 75248 Paris, Cedex 05, France; [4]Medical Research Council, Laboratory for Molecular Cell Biology and Cell Biology Unit, Department of Anatomy and Developmental Biology, University College London, Gower Street, London, WC1E 6BT, United Kingdom; [5]Cancer Research UK, London Research Institute, 44 Lincoln's Inn Field, London, WC2A 3PX, United Kingdom.
[6]These authors contributed equally to this work.
[7]Correspondence should be addressed to J.-R.H. (e-mail: jean-rene.huynh@curie.fr)

Received 14 November 2008; accepted 10 February 2009; published online 10 May 2009; DOI: 10.1038/ncb1874

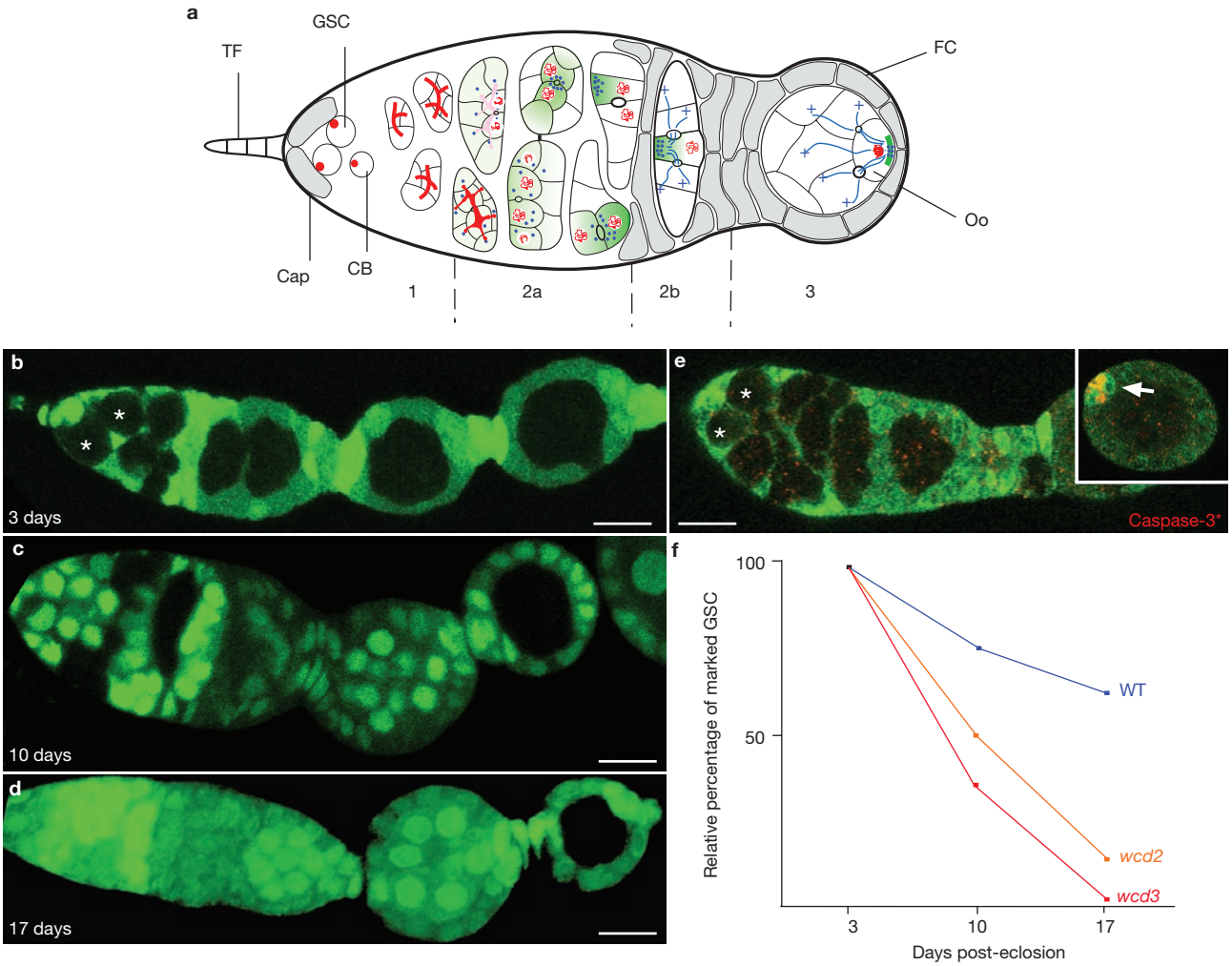

Figure 1 *Wcd* is required for GSC self-renewal. (**a**) *Drosophila* early oogenesis. An egg chamber comprises 16 germline cells surrounded by follicle cells (FC). The germarium is divided into 4 regions along the anterior–posterior axis (1, 2a, 2b, 3). GSCs reside at the tip of the germarium (left) in a microenvironment created by cap cells (Cap) and terminal filament cells (TF). GSCs produce cytoblasts, which divide four times and generate germline cysts of 16 cells connected by ring canals. The GSCs and cystoblasts contain a spectrosome (red circles), which develops into a branched fusome orienting cystoblast divisions. In region 2a, the synaptonemal complex (SyC, red lines) forms in the 2 cells with 4 ring canals (the pro-oocytes) as they enter meiosis. The SyC then appears transiently in the 2 cells with 3 ring canals, before becoming restricted to the pro-oocytes. By region 2b, the oocyte (Oo) is selected, and is the only cell to remain in meiosis. In region 2a, cytoplasmic proteins, mRNAs, mitochondria (green) and centrosomes (blue circles) accumulate progressively at the anterior of the oocyte. In region 2b, the minus ends of the microtubules are focused in the oocyte, and the plus ends extend through the ring canals into the nurse cells. The follicle cells (grey) start to migrate and surround the germline cells. As the cyst moves to region 3, the oocyte adheres to the posterior follicle cells and repolarizes along its anterior–posterior axis, with the microtubules (MT) minus ends and specific cytoplasmic components now localized at the posterior cortex. (**b**–**e**) *wcd* cells are labelled by the lack of GFP, in green. *wcd* GSCs (asterisks) can frequently be observed 3 days after hatching (**b**) but become rarer and rarer at 10 (**c**) and 17 (**d**) days after hatching. No activated caspase-3 (in red) is observed in *wcd* GSCs (**e**, asterisks). Endogenous apoptosis in polar cells serves as a positive control (arrow). (**f**) Relative percentage of negatively marked GSCs observed at 3, 10 and 17 days after hatching. The loss rate of wcd^2 and wcd^3 GSCs is more pronounced than that of wild-type (WT) GSCs. Scale bars, 10 μm.

described in yeast, its regulation in specific cell types and its involvement in cell differentiation remain unclear in multicellular organisms.

RESULTS

Wcd is essential for GSC maintenance

Screening for mutations affecting early oogenesis with the FLP/FRT system[20], we found one line that showed a marked decrease in the production of mutant clones in aged flies. We named this mutant *wicked*[1] (wcd^1) because of the severity of the phenotype. We identified and generated two additional alleles (see Methods), wcd^2 and wcd^3, and observed the same phenotype with all three mutations. To test the involvement of *wcd* in GSC self-renewal, we generated negatively labelled wild-type or *wcd* GSCs and compared their rates of loss (Fig. 1b). We observed a gradual decrease of negatively labelled WT GSCs, reflecting their described half-life (Fig. 1f, Table 1). In contrast, the rate of loss of *wcd* GSCs was much more pronounced: after seventeen days, *wcd* GSCs were recovered in 2.8% of wcd^2 ($n = 355$) and in 0.4% of wcd^3 mosaic germaria ($n = 233$) (Fig. 1b–d, f). This loss of mutant GSCs could have been caused by increased cell death or premature differentiation. To distinguish between these possibilities, we used markers of apoptosis in *wcd* GSCs and did not detect DNA fragmentation or activation of caspase-3 ($n = 58$; Fig. 1e), indicating that GSC loss was not the result of apoptosis. Instead, our data

Table 1 Marked GSC clones

Genotypes	3 days	10 days	17days
Wild Type *(FRTG13)*	21.5%/100% (265)	16.1%/75% (380)	12.2%/58% (287)
wcd^{2}	17.8%/100% (157)	9.1%/51% (395)	2.8%/16% (355)
wcd^{3}	17.4%/100% (149)	6.1%/35% (396)	0.4%/2% (233)

Data are expressed as the percentage of germaria with at least one GFP-negative stem cell over the percentage of germaria normalized at the first time-point. The numbers in parentheses are the total numbers of germaria scored for each time-point.

indicate that *wcd* GSCs differentiated prematurely. *Wcd* thus seems to be essential in the balance between GSC self-renewal and differentiation.

Wcd encodes the *Drosophila* homologue of UTP18, a conserved nucleolar protein

We mapped the *wcd*^{1} mutation to a substitution from Asp to Val in position 277 of the *l(2)k07824* gene, herein named *wicked* (Fig. 2a). *Wcd* is a 1.5 kb gene with no intron, encoding an evolutionarily conserved protein consisting of 506 amino acids that is predicted to contain four WD40 repeats (Supplementary Information, Fig. S1a). Its human homologue WDR50 was identified in a proteomics study of nucleoli[21]. The yeast homologue, U3 snoRNA-associated protein18 (UTP18), is part of a large ribonucleoprotein complex required for 18S rRNA biogenesis[22]. We identified and generated two null alleles, *wcd*^{2} and *wcd*^{3} (Fig. 2a; Supplementary Information, Fig. S1c–e). Transgenic lines expressing an RFP::Wcd fusion protein in *wcd*^{2} clones completely rescued GSC self-renewal and germline cyst development (Fig. 2b), confirming the involvement of *wcd* at these steps and showing the functionality of RFP::Wcd. The localization of Wcd was determined using an antibody directed against the amino-terminal half of the protein (Supplementary Information, Fig. S1a–b). Both endogenous Wcd and its GFP/RFP-tagged versions were distributed within the nucleus, although not evenly (Supplementary Information, Fig. S2 shows a comparison of the distributions of endogenous Wcd and GFP/RFP::Wcd expressed in the presence or absence of endogenous protein). Wcd was localized in two nuclear sub-regions where DNA staining was weak or absent, both in germ and follicle cells (Supplementary Information, Fig. S2c–e and data not shown). In the oocyte, Wcd was present throughout the germinal vesicle (Supplementary Information, Fig. S2a2). Double-labelling with the nucleolar marker Fib showed perfect colocalization with the main pool of Wcd (Fig. 2d, d′′; Supplementary Information, Fig. S3g1–3), demonstrating that Wcd is nucleolar. However, we found that Wcd did not colocalize with Fib in the Cajal body (Supplementary Information, Fig. S3g1–3). The second and smaller pool of Wcd colocalized with LSM11 (Fig. 2e, e′′) indicating that it is part of the histone locus body, which contains the U7 small nuclear RNP (snRNP) and the stem-loop binding protein (Slbp), which are both required for the 3′-end cleavage of histone pre-mRNA[23–25]. However, in contrast to *wcd* mutations, complete deletions of the U7 snRNA and null mutations in *Slbp* affect only late stages of oogenesis[23,24]. We thus focused on the function of nucleolar Wcd.

Wcd is a functional component of the *Drosophila* U3 sno-RNP required for pre-rRNA maturation.

To test whether Wcd could be part of the U3 snoRNP, we performed immunoprecipitation experiments on ovarian extracts using the Fib antibody. Western blot analysis after immunoprecipitation showed that Wcd is present in a complex with Fib (Fig. 3a). This was confirmed using an anti-Wcd antibody for immunoprecipitation and revealing the presence of Fib within the Wcd-containing complex (Fig. 3b). By contrast, no Fib was detected when immunoprecipitation was carried out using the Wcd pre-immune serum. Wcd and Fib are thus part of a nucleolar complex *in vivo*. To analyse whether the Wcd-containing complex is associated with the U3 snoRNA, we performed similar immunoprecipitation experiments followed by northern blotting using a probe directed against the U3 snoRNA. A specific band the size of U3 was observed after immunoprecipitation with the anti-Wcd antibody, indicating that Wcd is part of the U3 snoRNP (Fig. 3c). Following the same approach using a probe directed against the first ITS of the pre-rRNA, we observed that the pre-rRNA can also be found in a complex with Wcd, consistent with a role in its maturation (Fig. 3c). To test this, we treated S2 cells with dsRNA directed against the first half of the *wcd* mRNA, which resulted in efficient knockdown (Fig. 3e). We then performed northern blot analysis using probes directed against regions within the ETS, ITS1, ITS2, 18S and 28S sequences of the pre-rRNA (Fig. 3f and data not shown). The sequential cleavages of the pre-rRNA led to a series of intermediates, designated a–e (Fig. 3d); two alternative processing pathways, A and B, have been described previously[26]. We observed an accumulation of the long form of the pre-rRNA in *wcd* RNAi treated cells compared with the control (Fig. 3f), indicating defects in the early maturation steps. We also noticed a decrease in the amounts of intermediate b and an accumulation of intermediate d (Fig. 3f). These results strongly suggest that Wcd is required for cleavage 2 and/or 3 of processing pathway A. They also support the hypothesis that, when pathway A is compromised, maturation occurs through pathway B[27]. Together these experiments show that Wcd is a functional component of the U3 snoRNP required for pre-rRNA maturation.

A fraction of Wcd forms particles segregating asymmetrically into the GSCs and pro-oocytes

This general function of Wcd contrasts with its specific requirement for GSC self-renewal. To investigate this paradox, we studied the localization of Wcd during divisions of GSCs and germline cysts. Surprisingly, in metaphase Wcd concentrated as one or more bright cytoplasmic dots that segregated into the future stem cell during anaphase (Fig. 4a–d). We observed the same behaviour on fixed samples expressing Wcd::GFP (Fig. 4a, a′) or the endogenous Wcd (n = 20, Fig. 4b; Supplementary Information, Fig. S3b–f). To further analyse the distribution of Wcd during mitosis, we devised an experimental set-up to image dividing GSCs within their niche *ex vivo* (see Methods). Upon nuclear envelope breakdown, bright dots of Wcd formed and moved to the metaphase plate on the side of the future GSC and then preferentially segregated into the GSC (n = 6, Fig. 4c1–3, d1–3; Supplementary Information, Movies 1, 2). Smaller dots localizing in the cytoblast were also visible. Fluorescence of Wcd::GFP in particles in the GSC and in the cytoblast was measured and the ratio of these quantities calculated: 7 (6.9 ± 2.5) times more particles segregated into the GSC than into the cytoblast (Supplementary

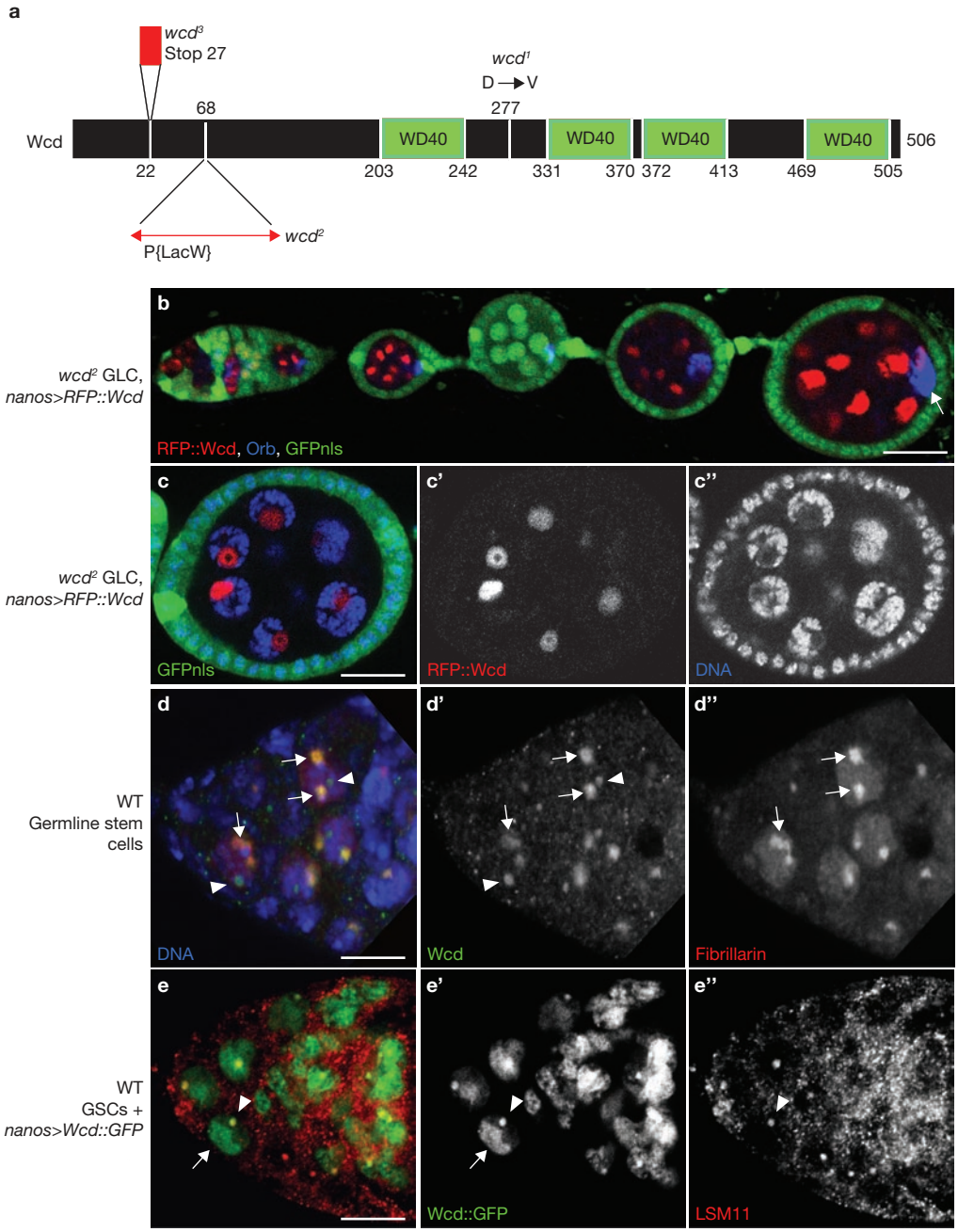

Figure 2 *Wcd* encodes a nucleolar protein containing four WD40 motifs. (**a**) Schematic representation of the Wcd protein (black bar). The *wcd*^{1} mutation leads to an amino acid substitution (Asp to Val) in position 277. The *wcd*^{2} mutation corresponds to a lethal transposable element insertion 68 base pairs downstream of the start site. The *wcd*^{3} mutation results from the imprecise excision of this transposable element, which leads to the presence of a stop codon at position 27. (**b**, **c**) *wcd*^{2} mutant cells are labelled by the lack of GFP, in green. The expression of RFP::Wcd, in red, was driven within *wcd*^{2} germline clones (GLC) using *nanos*–GAL4. (**b**) Expression of RFP::Wcd leads to a complete rescue of the growth phenotype. In addition, Orb, in blue, is correctly relocalized to the posterior of the oocyte (arrow). (**c**, **c**′′) RFP::Wcd (red in **c** and white in **c**′) accumulates in nuclear regions where the DNA staining (blue in **c** and white in **c**′′) is weak or absent. (**d**–**d**′′) The endogenous Wcd protein is green in **d** and white in **d**′. The nucleolar marker Fib is red in **d** and white in **d**′′. Fib overlaps perfectly with the main pool of Wcd (arrows) but a small fraction of Wcd resides in another nuclear sub-compartment (arrowheads). (**e**–**e**′′) Wcd–GFP is green in **e** and white in **e**′. The HLB marker LSM11 is red in **e** and white in **e**′′. The main pool on Wcd::GFP is nucleolar (arrow), whereas the small pool of Wcd::GFP colocalizes with LSM11 (arrowhead). Scale bars, 20 μm (**b**, **c**) and 4 μm (**d**, **e**)

Information, Fig. S4a). However, these particles represent only a fraction of the total amounts of Wcd::GFP (Supplementary Information, Fig. S5b). As GSCs and cytoblasts have similar sizes immediately after mitosis[14], the ratio of the total amounts of Wcd::GFP in the GSC and cytoblast is marginally above 1 (Supplementary Information, Fig. S4c), although the localization of Wcd::GFP is clearly asymmetric.

We further found that Wcd forms particles segregating preferentially into the two pro-oocytes during germline cyst divisions (Wcd::GFP in Fig. 4e1–4, f1–3; Supplementary Information, Movies 3, 4; endogenous Wcd in Supplementary Information, Fig. S3b1, 2). Our live-imaging

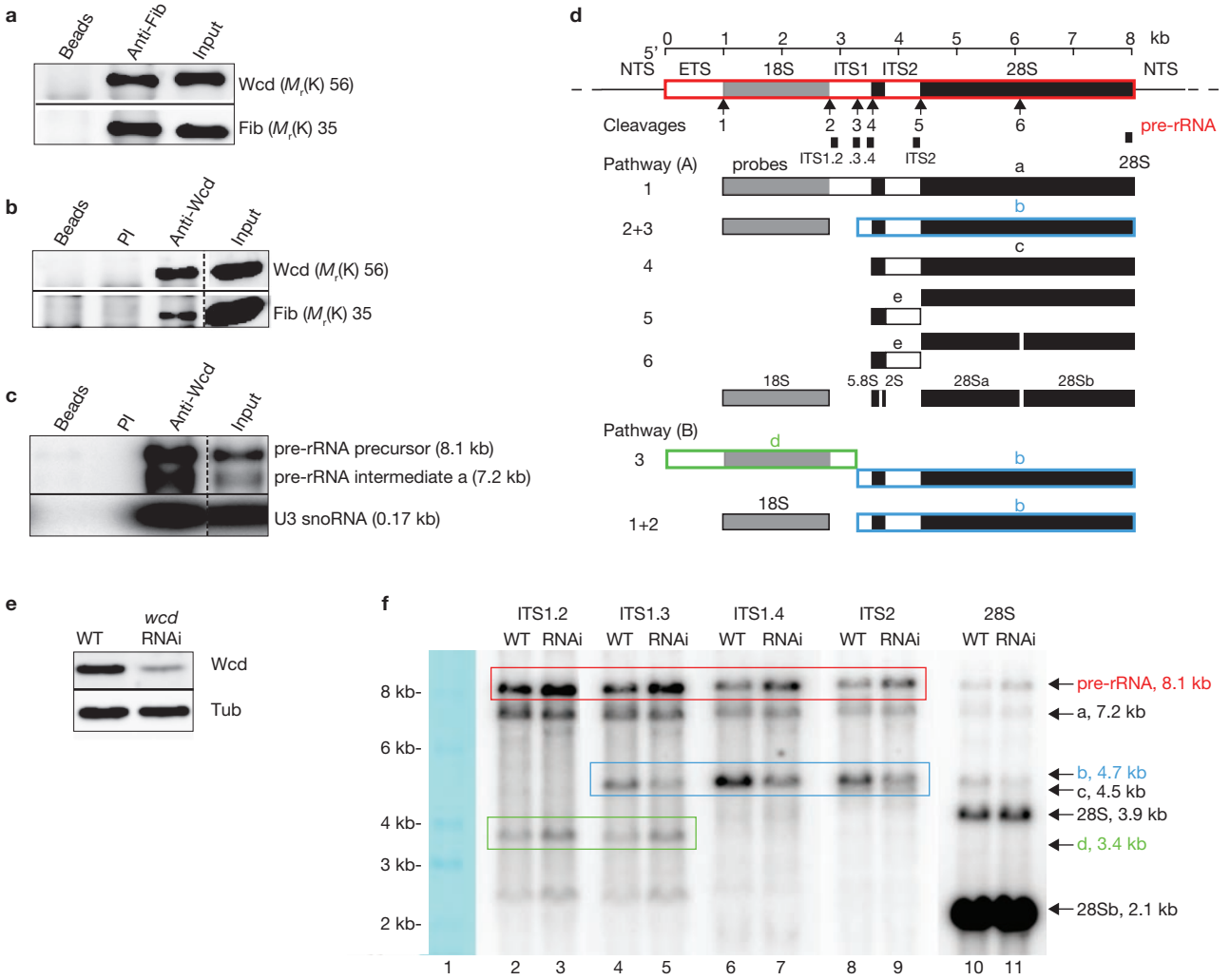

Figure 3 Wcd is a functional component of the U3 snoRNP required for pre-rRNA maturation. (**a**–**c**) Immunoprecipitation performed on ovarian extracts using anti-Fib (**a**) or anti-Wcd antibodies (**b**, **c**). PI, pre-immune serum. Wcd and Fib can be specifically co-immunoprecipitated (**a**, **b**). Western-blot analysis of the immunoprecipitate using anti-Wcd (upper panel) or anti-Fib (lower panel) antibodies. Northern-blot analysis of the immunoprecipitate using a radiolabelled probe directed against the pre-rRNA (**c**, top panel) or against the U3 snoRNA (**c**, bottom lane). A complex containing Wcd, the pre-rRNA and the U3 snoRNA can be specifically co-immunoprecipitated using anti-Wcd antibody (bottom lane). Data in the upper and lower gels (**a**, **b**) and top and middle panels (**c**) are from two different gels. Dashed lines in **b** and **c** indicate that lanes from the same gel have been juxtaposed. (**d**) Schematic representation of the pre-rRNA processing pathways A and B (adapted from Long and Dawid[26]). The top line shows the structure of the pre-rRNA; the ETS and ITS are shown in white, the 18S subunit in grey and the 5.8S, 2S and 28S subunits in black. The cleavage sites are numbered from 1 to 6. The different maturation intermediates indicated by the letters a–e. The probes used for northern blot analysis are represented as black boxes. (**e**) Western blot analysis of *wcd* RNAi-treated S2 cells, using anti-Wcd antibody (upper panel) or anti-tubulin (Tub) antibody (lower panel). *wcd* RNAi treatment resulted in an efficient and specific knockdown of Wcd (compare wild-type (WT) cells, left lane, with RNAi treated cells in the right lane. (**f**) Northern blot analysis of *wcd* RNAi-treated S2 cells using the probes described in **d**. Arrows on the right highlight the pre-rRNA and the different maturation intermediates. Knockdown of Wcd leads to an increase in the amount of pre-rRNA (compare lanes 3, 5, 7, 9 with lanes 2, 4, 6, 10), an increase in the amount of the intermediate d (compare lanes 3 and 5 with lanes 2 and 4) and a decrease in the amount of intermediate b (compare lanes lanes 5, 7, 9 with lanes 4, 6, 8). The 28S probe served as an internal loading control. Full gel scans for **a**–**c**, **e** and **f** can be seen in Supplementary Information, S7.

analysis demonstrates that a pool of Wcd forms asymmetrically segregating particles during the GSC and germline cyst mitosis and reveals an intrinsic asymmetry of the GSC division.

Wcd asymmetric localization is independent of the Dpp signal

The asymmetric outcome of the GSC division is controlled mainly by Dpp, which is secreted by the niche and promotes GSC fate[28–30]. Accordingly, overactivation of the Dpp pathway induces an overproliferation of GSCs or GSC-like cells in 'stem cell tumours' filling up the germarium. To test whether the asymmetric distribution of Wcd depends on the Dpp pathway, we expressed an activated form of the Dpp receptor Thickveins (Tkv) in the GSCs[29,31]. Germaria were filled with single cells dividing away from the niche with random orientations (Fig. 5a). Our movies showed that Wcd::GFP was still segregating into only one of the two daughter cells ($n = 8$, Fig. 5d1–3; Supplementary Information, Movies 5, 6). This asymmetry was not undirected as Wcd::GFP always localized into the cell retaining the original spectrosome: 10.5 ± 5.5 times more Wcd::GFP segregated into that cell ($n = 22$, Fig. 5b, c; Supplementary Information, Fig. S4a), representing

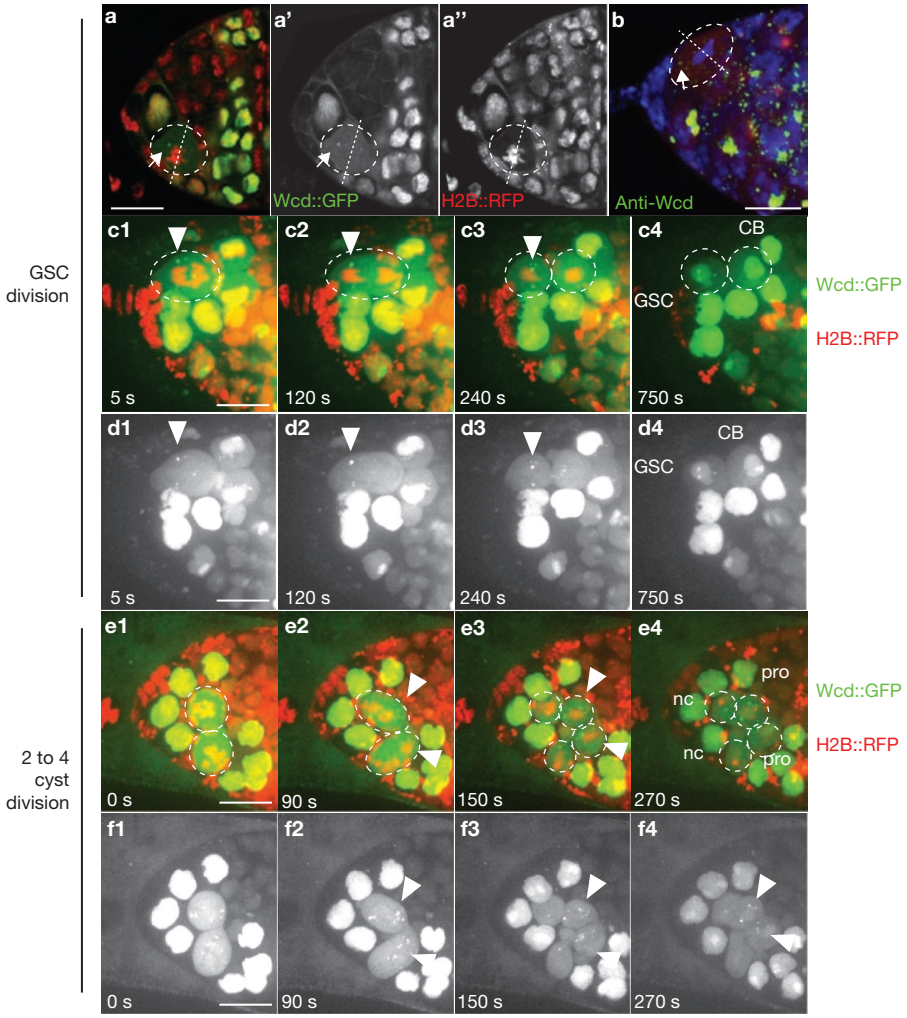

Figure 4 Wcd is asymmetrically segregated upon GSC mitosis. (**a**, **c**, **e**) Wcd::GFP is in green. The DNA marker histoneH2B::RFP (H2B::RFP) is in red. The dividing GSC is highlighted by a white dashed circle (**a**–**c**) and the orientation of the metaphase plate is indicated by a white straight dashed line (**a**, **b**). Wcd::GFP forms a dot upon GSC division (arrow), which is located on the side of the future GSC (**a**). Single channels are shown for Wcd::GFP (**a**′) and H2B::RFP (**a**′′). (**b**) Wcd is in green and DAPI staining is in blue. The endogenous Wcd protein also segregates asymmetrically as a dot upon GSC division (arrow), which is located on the side of the future GSC. (**c**, **d**) *Ex-vivo* imaging of GSC division. Time (s) is indicated at the bottom left of each panel. The Wcd::GFP channel is shown on its own in **d**. Soon after nuclear envelope breakdown, Wcd::GFP forms a bright dot (arrowhead) that segregates into the new GSC. Once the two daughter cells have re-formed, the dot relocalizes to the nucleus of the GSC and cytoblast. (**e**, **f**) *Ex-vivo* imaging of germline cyst division, which leads to the formation of a four-cell cyst. The dividing cyst is highlighted by a white dashed line (**e**). The Wcd::GFP channel is shown on its own in **f**. Soon after nuclear envelope breakdown, Wcd::GFP forms several bright dots that are preferentially segregated into two of the four daughter cells (arrowheads), which we identify as the two pro-oocytes (pro) based on their positions. nc: nurse cells. Scale bars, 4 μm.

3 ± 1.6% of the total amounts of Wcd::GFP. Therefore, although the outcome of division is symmetric in terms of fate, the mitosis itself is asymmetric regarding the spectrosome and the distribution of Wcd::GFP[32].

Wcd particles segregate asymmetrically into neural stem cells and are required for stem cell growth

Overall, Wcd distribution is similar to the partially (as opposed to all or nothing) asymmetric behaviour of the fusome during GSC and cyst divisions in wild-type and mutant conditions. To test whether the asymmetric segregation of Wcd is germline-specific or whether it occurs in other cell types, we analysed Wcd dynamics during neural stem cell (NSC) divisions, which are well-characterized asymmetric divisions with no fusome[33]. Larval neuroblasts are NSCs generating dozens of neurons in the fly central nervous system after repeated rounds of self-renewing asymmetric divisions during which a new neuroblast and a smaller ganglion mother cell (GMC) are generated. The GMC divides once more to produce two ganglion cells. *Ex-vivo* imaging of neuroblast division revealed dots of Wcd::GFP reproducibly segregating into the neuroblast (13/16, Fig. 6a1–3; Supplementary Information, Movies 7, 8). The dots formed during early anaphase, later than in the GSCs, and had segregated into neuroblasts by telophase. Five (5.38 ± 3.3) times more particles of Wcd::GFP segregated into neuroblasts than into GMCs (Supplementary Information, Fig. S4a), representing 1.4 ± 1% of the total amount of Wcd::GFP (Supplementary Information, Fig. S4b). Similar temporal and spatial behaviour was found for the endogenous protein (Supplementary Information, Fig. S3d1, 2). Wcd also segregated asymmetrically during mitosis of the precursor cell of the bristle lineage (pI cell), albeit infrequently (2/19, Supplementary Information, Fig. S5, Movie 9). These results show that Wcd can localize

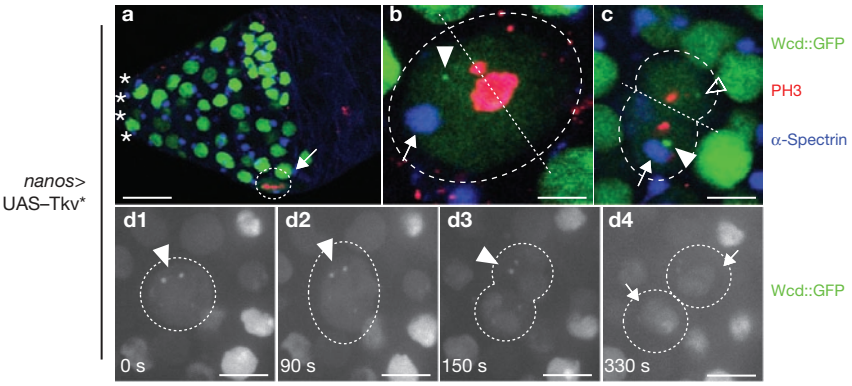

Figure 5 Asymmetric segregation of Wcd is independent of the Dpp signal. (**a**–**d**) Overexpression of activated Tkv under the control of the *nanos*–GAL4 driver. The mitotic marker phospho-histoneH3 (PH3) is in red and the spectrosome marker α-Spectrin is in blue (**a**–**c**). The orientation of the metaphase plate is indicated by a white straight dashed line (**b**, **c**). A GSC-like cell (highlighted by a white dashed circle) dividing at a distance from the niche (**a** arrow). Asterisks highlight the niche cells. Metaphase (**b**): Wcd::GFP segregates asymmetrically upon GSC-like cell division (arrowhead), together with the spectrosome (arrow). Anaphase (**c**): asymmetric segregation of Wcd::GFP as a dot (arrowhead) together with the spectrosome (arrow). A smaller dot of Wcd::GFP also segregates into the other daughter cell (empty arrowhead). *Ex-vivo* imaging of GSC-like division (**d**). Dots of Wcd::GFP form soon after entry into mitosis (arrowheads) and disappear in late telophase when the nuclei of the daughter cells re-form (arrows). Scale bars, 5 μm (**a**), 0.5 μm (**b**) and 0.7 μm (**c**, **d**)

asymmetrically in the absence of a fusome. More importantly, the unequal segregation of a U3snoRNP component is a conserved feature in germ and neural cells. Furthermore, Wcd segregates into the larger and/or self-renewing cell in all cases.

We analysed the requirement of *wcd* in ventral nerve cord neuroblasts using the MARCM system[34] (Fig. 6b, c). We found that *wcd* neuroblasts sequentially produced early-born Chinmo$^+$ ganglion cells and late-born Br-C$^+$ ganglion cells[35] (Supplementary Information, Fig. S6). However, *wcd* neuroblasts generated only half the number of ganglion cells produced by wild-type NSCs ($n = 20$; Fig. 6d). To test whether this reduction reflected an increase in cell death, we performed activated caspase-3 stainings and found no difference between *wcd* and wild-type clones (data not shown). We also expressed the inhibitor of apoptosis p35 (ref. 36) in wild-type and mutant MARCM clones and found that *wcd* neuroblasts still generated about half the number of ganglion cells produced by wild-type neuroblasts ($n = 22$; Fig. 6d). We then investigated whether this phenotype was associated with changes in neuroblast size by measuring the volume of wild-type and mutant neuroblasts. On average, *wcd* neuroblasts were half the size of wild-type neuroblasts ($n = 20$, Fig. 6e). Wcd is thus required for NSC proliferation and growth.

DISCUSSION

We identified *wcd* as a *Drosophila* gene required for stem cell self-renewal. We characterized its molecular function and validated our results *in vivo* in a multicellular organism. Live-imaging of single stem cells and analysis of fixed samples revealed asymmetric segregation of Wcd particles upon mitosis both in GSCs and NSCs. Overall, our results show that the regulation of cell size by ribosome synthesis is an important parameter for stem cell maintenance and function.

Large and/or rapidly dividing stem cells face the challenge of sustaining a high growth rate to maintain their size and function over long periods of time. They must, therefore, be particularly sensitive to mutations that decrease ribosome production, such as *wcd*. Their growth must also be tightly regulated, as mutations that increase ribosome biogenesis can cause stem cells to overproliferate and form tumours[37]. For example, mutations in the *brat* gene induce overproliferation of certain NSCs and the formation of tumours in *Drosophila* brain[38–41]. Brat was shown to repress growth by acting in part through the repression of ribosome biogenesis[40,42]. Interestingly, Brat segregates asymmetrically into pIIb cells and GMCs during divisions of pI cells and NSCs, respectively, which is opposite to Wcd in both cases. Similarly, mutations in the *brat* homologue *mei-P26* generate tumours specifically in the germarium[43]. Mei-P26 expression is low in GSCs and high in differentiating germline cysts, where it restricts growth[14]. In the absence of *Mei-P26*, cystocytes grow abnormally and fail to differentiate. The current model is that *brat* and *mei-P26* regulate cell and nucleolus size in stem cell lineages by inhibiting ribosome biogenesis in the differentiating daughter cells[14]. Our results suggest a twofold process in which ribosome formation is decreased in the smaller differentiating cell and increased in the larger and/or self-renewing cell.

An alternative possibility is that Brat, Mei-P26 or Wcd may associate with cell-type-specific ribosomal proteins or ribosome biogenesis pathways performing specialized functions, as shown in yeast[44]. Support for this hypothesis comes from microarray analysis of female GSCs in *Drosophila*, which showed enrichment in specific isoforms of ribosomal proteins and regulators of ribosome biogenesis[32]. Neither alternative, based respectively on quantitative or qualitative differences in the ribosome biogenesis pathway, is exclusive.

Is the asymmetric segregation of Wcd responsible for differential growth? To address this question, we overexpressed Wcd in the germline and nervous system, but did not observe any phenotype, suggesting that overexpression of Wcd is insufficient to induce overgrowth (data not shown). However, there are several explanations for this result, limiting the interpretation of this kind of experiment. First, although Wcd is required for growth, it is probably not an essential limiting factor as mutant GSCs and NSCs were observed several days after the loss of *wcd*. Second, the localization of Wcd is not an all-or-nothing asymmetry as is the segregation of Numb in the nervous system[45]. Wcd is expressed in every cell and only a small fraction of Wcd segregates preferentially into the stem cell during mitosis (Supplementary Information, Fig. S4b). Third, even if Wcd levels were increased in the cystoblast/GMC, endogenous Mei-P26

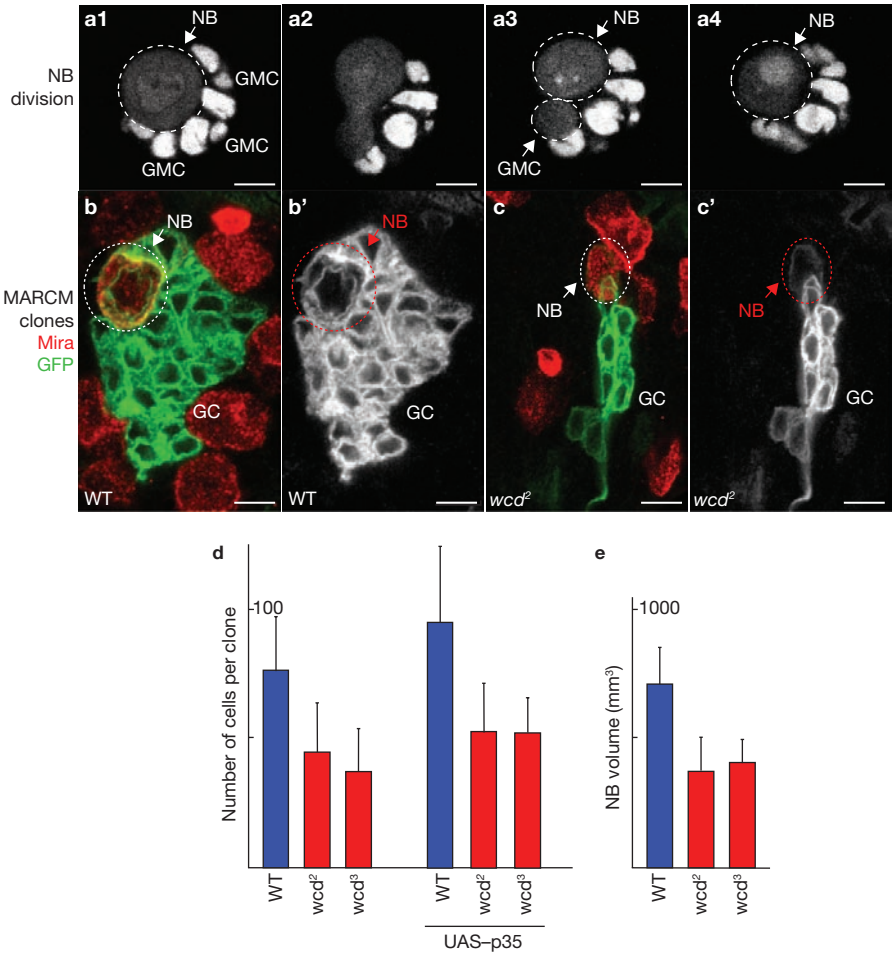

Figure 6 Wcd is asymmetrically segregated upon neuroblast division in the larval central nervous system and is required for neural stem cell proliferation and growth. (**a**) Wcd::GFP is in white. (**b**, **c**) Membrane-associated GFP positively labels the clones in green. The neuroblast (NB) marker Miranda (Mira) is shown in red. (**a**) An *ex-vivo* NB (indicated by an arrow) with several of its daughter ganglion mother cells (GMCs). Wcd::GFP forms two large dots (**a3**, arrowhead), which are inherited asymmetrically by the NB (white circle). The nucleolus then re-forms at telophase (**a4**). (**b**) A GFP-labelled wild-type (WT) NB, (white circle) and part of its progeny (GC). (**b**′) GFP channel. (**c**) A GFP-labelled *wcd*^{2} NB and part of its progeny (GC). (**c**′) GFP channel. (**d**, **e**) *wcd* mutant NBs produce fewer GCs (**d**) and are smaller (**e**) than WT NBs. (**d**) Average number of GCs observed in WT (blue bar) and *wcd* mutant clones (red bars) when apoptosis can occur (**d**, left panel, $n = 20$) or when apoptosis is inhibited by overexpression of the caspase inhibitor p35 (UAS–p35, **d**, right panel, $n = 22$). (**e**) Measurement of the volume of WT (blue bar) and *wcd* mutant (red bars) NBs ($n = 20$). Data are mean ± s.d.; scale bars, 10 μm.

and Brat would still be present and repress ribosome synthesis[14,40]. Overall, we have shown that Wcd is required for stem cell maintenance; however, whether its asymmetric localization has an instructive role is unclear and difficult to test experimentally. Nevertheless, our work and other studies published recently[14,40] support the idea that differential ribosome biogenesis *per se* regulates asymmetric growth and self-renewal in stem cell lineages. There is a clear correlation between Wcd, Brat and Mei-P26 distribution and cell size. Wcd segregates into the larger GSC, NSC and pIIa cell. In contrast, Brat localizes into the smaller GMC and pIIb cell[38–41]. Similarly, Mei-P26 is highly expressed in the small cystocytes and at low levels in the larger GSCs[14]. Finally, Wcd does not form particles and is partitioned equally in symmetrically dividing follicle cells (Supplementary Information, Fig. S3h1–3, Movie 10). Increasing ribosome biogenesis is sufficient to induce differentiating cells to form tumours. In *brat* and *mei-P26* mutants, the nucleolus enlarges, suggesting an increase in ribosome formation[40]. Consequently cells overgrow and fail to exit the cell cycle and to differentiate, leading to the formation of tumours. Decreasing ribosome biogenesis triggers premature stem cell differentiation: the absence of Wcd induces severe rRNA maturation defects and leads to the differentiation of GSCs. Similarly, overexpression of Mei-P26 reduces nucleolus size and triggers stem cell loss[14,40].

Another question arising from our work is whether the differential segregation of Wcd is a cause or a consequence of the asymmetry of stem cell division. In the germline, the main source of asymmetry is the Dpp signal sent by the niche, and expression of activated Tkv is sufficient to transform the asymmetric GSC division into one producing two identical GSCs or GSC-like cells[29,31]. Under these conditions, Wcd and the spectrosome co-segregated preferentially into one cell, demonstrating that their asymmetric distribution is independent of Dpp signalling. This reveals an intrinsic asymmetry of GSC or GSC-like divisions independent of the niche's signals and adhesion. It also shows that artificially activating the Dpp pathway is sufficient to induce both daughter cells to become GSCs, regardless of the spectrosome and Wcd asymmetry. This suggests that the extrinsic signals from the niche have a primary influence over intrinsic factors on cell fate in the ovary. This

conclusion may also hold true under specific wild-type conditions, as the fusome is still unequally partitioned when a GSC divides perpendicular to the anterior-posterior axis so that both daughter cells remain in the niche and become stem cells[9].

Better understanding of stem-cell-driven regeneration is likely to arise from live-imaging of single stem cells within their microenvironment over long periods of time, with a good spatial and temporal resolution[46]. We show the possibility of maintaining and imaging *ex vivo* the entire ovarian niche for several hours. This has allowed us to uncover a transient asymmetry in the segregation of Wcd, which would have been difficult to detect in fixed tissues. We believe that this technique will allow new questions to be addressed and, together with a combination of genetic and biochemical approaches, will help uncover essential processes underlying the extraordinary properties of stem cells.

METHODS

Methods and any associated references are available in the online version of the paper at http://www.nature.com/naturecellbiology/

Note: Supplementary Information is available on the Nature Cell Biology website.

ACKNOWLEDGMENTS

We are especially grateful to Danièle Hernandez-Verdun, Bruno Bello, Frank Hirth, Andrew Vaughan and the Imaging facilities at IJM for experimental advice; to Danièle Hernandez-Verdun, Acaimo Gonzalez-Reyes, Antoine Guichet, Juliette Mathieu, Emily Richardson and Ralph Neumuller for critical reading. We are also grateful for reagents provided by Danièle Hernandez-Verdun, Joe Gall, Acaimo Gonzalez-Reyes, Fumio Matsuzaki, Christophe Antoniewski, Antoine Guichet, Christian Lehner, Alex Gould, Tzumin Lee, Barry Thompson, DHSB (Iowa University) and Bloomington *Drosophila* Stock center. We wish to thank Franck Pichaud (MRC-LMCB, UCL) in whose lab part of this work was performed. This work was funded by grants to J.R.H. (CNRS, ARC # 3802, and ANR # 06-JCJC-0092-01), P.F. (ARC post-doctoral fellowhip and EMBO long term fellowship), CM (CNRS), J.A.L. (CNRS, ARC# 3802) Ch.M. and Y.B. (CNRS, Curie).

COMPETING FINANCIAL INTERESTS

The authors declare no competing financial interests.

Published online at http://www.nature.com/naturecellbiology/
Reprints and permissions information is available online at http://npg.nature.com/reprintsandpermissions/

1. Birnbaum, K. D. & Sanchez Alvarado, A. Slicing across kingdoms: regeneration in plants and animals. *Cell* 132, 697–710 (2008).
2. Morrison, S. J. & Spradling, A. C. Stem cells and niches: mechanisms that promote stem cell maintenance throughout life. *Cell* 132, 598–611 (2008).
3. Gilboa, L. & Lehmann, R. How different is Venus from Mars? The genetics of germ-line stem cells in *Drosophila* females and males. *Development* 131, 4895–4905 (2004).
4. Wong, M. D., Jin, Z. & Xie, T. Molecular mechanisms of germline stem cell regulation. *Annu. Rev. Genet.* 39, 173–195 (2005).
5. Song, X. & Xie, T. DE-cadherin-mediated cell adhesion is essential for maintaining somatic stem cells in the *Drosophila* ovary. *Proc. Natl Acad. Sci. USA* 99, 14813–14818 (2002).
6. Xie, T. & Spradling, A. C. Decapentaplegic is essential for the maintenance and division of germline stem cells in the *Drosophila* ovary. *Cell* 94, 251–260 (1998).
7. Fichelson, P. & Huynh, J. R. Asymmetric divisions of germline cells. *Prog. Mol. Subcell. Biol.* 45, 97–120 (2007).
8. Deng, W. & Lin, H. Spectrosomes and fusomes anchor mitotic spindles during asymmetric germ cell divisions and facilitate the formation of a polarized microtubule array for oocyte specification in *Drosophila*. *Dev. Biol.* 189, 79–94 (1997).
9. Xie, T. & A, S. A niche maintaining germline stem cells in the *Drosophila* ovary. *Science* 290, 328–330 (2000).
10. de Cuevas, M., Lilly, M. A. & Spradling, A. C. Germline cyst formation in *Drosophila*. *Annu. Rev. Genet.* 31, 405–428 (1997).
11. Huynh, J. R. & St Johnston, D. The origin of asymmetry: early polarisation of the *Drosophila* germline cyst and oocyte. *Curr. Biol.* **14**, R438–449 (2004).
12. de Cuevas, M. & Spradling, A. C. Morphogenesis of the *Drosophila* fusome and its implications for oocyte specification. *Development* 125, 2781–2789 (1998).
13. Huynh, J. R. Fusome as a cell–cell communication channel of *Drosophila* ovarian cyst (Landes Biosciences, 2006).
14. Neumuller, R. A. *et al.* Mei-P26 regulates microRNAs and cell growth in the *Drosophila* ovarian stem cell lineage. *Nature* (2008).
15. Rudra, D. & Warner, J. R. What better measure than ribosome synthesis? *Genes Dev.* 18, 2431–2436 (2004).
16. Frescas, D., Guardavaccaro, D., Bassermann, F., Koyama-Nasu, R. & Pagano, M. JHDM1B/FBXL10 is a nucleolar protein that represses transcription of ribosomal RNA genes. *Nature* 450, 309–313 (2007).
17. Maaloe, O. & Kjedgaard, N. *Control of macromolecular synthesis*, (W. A. Benjamin, New York, 1966).
18. Boisvert, F. M., van Koningsbruggen, S., Navascues, J. & Lamond, A. I. The multifunctional nucleolus. *Nature Rev. Mol. Cell Biol.* 8, 574–585 (2007).
19. Matera, A. G., Terns, R. M. & Terns, M. P. Non-coding RNAs: lessons from the small nuclear and small nucleolar RNAs. *Nature Rev. Mol. Cell Biol.* 8, 209–220 (2007).
20. Xu, T. & Rubin, G. Analysis of genetic mosaics in developing an adult *Drosphila* tissues. *Development* 117, 1223–1237 (1993).
21. Scherl, A. *et al.* Functional proteomic analysis of human nucleolus. *Mol. Biol. Cell* 13, 4100–4109 (2002).
22. Dragon, F. *et al.* A large nucleolar U3 ribonucleoprotein required for 18S ribosomal RNA biogenesis. *Nature* 417, 967–970 (2002).
23. Godfrey, A. C. *et al.* U7 snRNA mutations in *Drosophila* block histone pre-mRNA processing and disrupt oogenesis. *RNA* 12, 396–409 (2006).
24. Lanzotti, D. J. *et al.* *Drosophila* stem-loop binding protein intracellular localization is mediated by phosphorylation and is required for cell cycle-regulated histone mRNA expression. *Mol. Biol. Cell* 15, 1112–1123 (2004).
25. Liu, J. L. *et al.* The *Drosophila melanogaster* Cajal body. *J. Cell Biol.* 172, 875–884 (2006).
26. Long, E. O. & Dawid, I. B. Alternative pathways in the processing of ribosomal RNA precursor in *Drosophila melanogaster*. *J. Mol. Biol.* 138, 873–878 (1980).
27. Giordano, E., Peluso, I., Senger, S. & Furia, M. *minifly*, a *Drosophila* gene required for ribosome biogenesis. *J. Cell Biol.***144**, 1123–1133 (1999).
28. Chen, D. & McKearin, D. Dpp signaling silences bam transcription directly to establish asymmetric divisions of germline stem cells. *Curr. Biol.* 13, 1786–1791 (2003).
29. Casanueva, M. O. & Ferguson, E. L. Germline stem cell number in the *Drosophila* ovary is regulated by redundant mechanisms that control Dpp signaling. *Development* 131, 1881–1890 (2004).
30. Song, X. *et al.* Bmp signals from niche cells directly repress transcription of a differentiation-promoting gene, bag of marbles, in germline stem cells in the *Drosophila* ovary. *Development* 131, 1353–1364 (2004).
31. Bolivar, J., Pearson, J., Lopez-Onieva, L. & Gonzalez-Reyes, A. Genetic dissection of a stem cell niche: the case of the *Drosophila* ovary. *Dev. Dyn.* 235, 2969–2979 (2006).
32. Kai, T., Williams, D. & Spradling, A. C. The expression profile of purified *Drosophila* germline stem cells. *Dev. Biol.* (2005).
33. Betschinger, J. & Knoblich, J. A. Dare to be different: asymmetric cell division in *Drosophila*, *C. elegans* and vertebrates. *Curr. Biol.* **14**, R674–685 (2004).
34. Lee, T. & Luo, L. Mosaic analysis with a repressible cell marker for studies of gene function in neuronal morphogenesis. *Neuron* 22, 451–461 (1999).
35. Maurange, C., Cheng, L. & Gould, A. P. Temporal transcription factors and their targets schedule the end of neural proliferation in *Drosophila*. *Cell* 133, 891–902 (2008).
36. Clem, R. J., Fechheimer, M. & Miller, L. K. Prevention of apoptosis by a baculovirus gene during infection of insect cells. *Science* 254, 1388–1390 (1991).
37. Al-Hajj, M. & Clarke, M. F. Self-renewal and solid tumor stem cells. *Oncogene* 23, 7274–7282 (2004).
38. Bowman, S. K. *et al.* The tumor suppressors Brat and Numb regulate transit-amplifying neuroblast lineages in *Drosophila*. *Dev. Cell* 14, 535–546 (2008).
39. Bello, B., Reichert, H. & Hirth, F. The brain tumor gene negatively regulates neural progenitor cell proliferation in the larval central brain of *Drosophila*. *Development* 133, 2639–2648 (2006).
40. Betschinger, J., Mechtler, K. & Knoblich, J. A. Asymmetric segregation of the tumor suppressor brat regulates self-renewal in *Drosophila* neural stem cells. *Cell* 124, 1241–1253 (2006).
41. Lee, C. Y., Wilkinson, B. D., Siegrist, S. E., Wharton, R. P. & Doe, C. Q. Brat is a Miranda cargo protein that promotes neuronal differentiation and inhibits neuroblast self-renewal. *Dev. Cell* 10, 441–449 (2006).
42. Frank, D. J., Edgar, B. A. & Roth, M. B. The *Drosophila melanogaster* gene brain tumor negatively regulates cell growth and ribosomal RNA synthesis. *Development* 129, 399–407 (2002).
43. Page, S. L., McKim, K. S., Deneen, B., Van Hook, T. L. & Hawley, R. S. Genetic studies of mei-P26 reveal a link between the processes that control germ cell proliferation in both sexes and those that control meiotic exchange in *Drosophila*. *Genetics* 155, 1757–1772 (2000).
44. Komili, S., Farny, N. G., Roth, F. P. & Silver, P. A. Functional specificity among ribosomal proteins regulates gene expression. *Cell* 131, 557–571 (2007).
45. Knoblich, J., Jan, L. & Jan, Y. Asymmetric segregation of Numb and Prospero during cell division. *Nature* 377, 624–627 (1995).
46. Schroeder, T. Imaging stem-cell-driven regeneration in mammals. *Nature* 453, 345–351 (2008).

METHODS

Fly strains and genetics. *wcd*^{1} was identified as a second site mutation on a chromosome also mutant for *shotgun*$^{P34-1}$ (DE-cadherin) during a pilot screen for mutations affecting the early steps of oogenesis (M. Jagut, L. Mihaila-Bodart, M. F. Alin, J. A. Lepesant and J. R. Huynh, in preparation). The two mutations were separated by outcrossing with w^{1118}, FRTG13 flies. *wcd*^{1} failed to complement *Df(2R)Exel6063* (Bloomington-7545) and *Df(2R)Exel7142* (Bloomington-7886). P-element insertions in the overlapping region were tested for complementation and the insertion *l(2)k07824* [*wcd*^{2}] inserted in the *CG7989* failed to complement *wcd*^{1}. *wcd*^{2} is a lethal P- element insertion 68 base pairs downstream of the start site (*l(2)k07824*$^{[k07824]}$, Fig. 2a). Given the insertion site, *wcd*^{2} was likely to be a null allele. This was confirmed by *in situ* hybridization and antibody staining in *wcd*^{2} mutant clones (Supplementary Information, Fig. S1c and data not shown). Precise excisions of *l(2)k07824* restored viability. Lethal $w^{-/-}$ excisions were screened by PCR for the presence of a fragment smaller than the wild-type *CG7989* locus. *wcd*^{3} is an imprecise excision of this P-element, resulting in the presence of a stop codon after amino acid 26 and a deletion of the downstream part of the gene (Fig. 2a). *wcd*^{3} is therefore very likely to be another null mutation (Supplementary Information, Fig. S1d, e1–4). The FLP/FRT system was used in combination of GFP for homozygous mutant clones selection. Germline clones were induced by heat-shock for 2 h at 37 °C for 2–3 consecutive days on third instar larvae. The following stocks were used: *y*, *w*, hsFLP12; FRT[G13]-ubiGFPnls; *nanos*–Gal4; H2B::RFP (gift from C. Lehner, University of Zurich, Switzerland); UASp–*tkv** (gift from A. Gonzalez-Reyes, CSIS-Universidad Pablo doe Olavide, Spain); w; *insc*-Gal4/+; *neuralized*^{P72}–Gal4 (ref. 47). To produce wild-type, *wcd*^{2} and *wcd*^{3} MARCM clones, the same number of *y w* hsFLP; FRTG13, *tubP*–GAL80/(CyO,*Act*GFPJMR1); *tubP*–GAL4, UAS–mCD8::GFP/TM6,*Tb,Hu* (gift from B.Bello, BioZentrum, Switzerland) virgins were crossed with the same number of FRTG13, FRTG13-*wcd*^{2} and FRTG13-*wcd*^{3} males respectively. To prevent apoptosis, the same experiments were carried using the following stocks: FRTG13; UAS-p35, FRTG13-*wcd*^{2};UAS–p35, and FRTG13-*wcd*^{3}; UAS–p35. Flies were left laying for 6 h at 25 °C and the egg collection was then kept for 22 h at 25 °C, followed by heatshock for 1 h at 37 °C. The heatshocked population of first instar larvae (aged between 0 and 6 h after hatching) was kept for four days at 25 °C. Wandering third instar larvae were then dissected and antibody staining performed. Quantifications of Wcd::GFP amounts were made using the ImageJ software. Cells were outlined manually and particles were defined as pixels above a threshold of fluorescence intensity. The amount of Wcd::GFP in particles is the sum of all pixel intensities above this threshold in each cell.

The volume of ventral nerve cord neuroblasts was measured using Miranda staining. Three-dimensional reconstructions and measurements were performed using Volocity software. Neuroblasts were first manually outlined at the level of their largest diameter and reconstructed in 3D. Only objects above a background threshold were analysed by the software. A noise-removing filter was applied and only objects bigger than 50 μm^3 were considered. Holes within such objects were filled and the total volume of pixel contained within these objects was measured, reflecting neuroblast size.

Rescue construct and fluorescently tagged proteins. A PCR fragment corresponding to the whole *wcd* cDNA sequence was amplified from the DGRC cDNA clone no. LD16320 using primers 5′-CACCATGAGTTCAGACGAGTCCAG-3′ and 5′-ATAACCCTTGAAGTACTTAAGCCTAAAG-3′ and cloned into the pENTR/D-TOPO Gateway entry vector using the pENTR directional TOPO cloning kit (Invitrogen). The *wcd* cDNA was then transferred to *Drosophila* transgenic expression vectors by LR recombination using the Gateway LR clonase II enzyme mix (Invitrogen). Destination vectors pPRW and pPWG were obtained from Terence Murphy's laboratory *Drosophila* Gateway Vector Collection at Carnegie Institution (http://www.ciwemb.edu/labs/murphy/Gateway%20vectors.html). The two resulting transgenic constructs consist of either mRFP N-terminal tagged (RFP::Wcd) or eGFP C-terminal tagged (Wcd::GFP) Wcd fusion proteins, both under the control of the UASp promoter, allowing GAL4-driven somatic and female germline expression. Transgenic lines were generated by standard methods.

Generation of anti-Wcd antisera. A PCR fragment was amplified from w^{1118} genomic DNA using primers 5′-AGCATGctcgagATGAGTTCAGACGAGTCC-3′ and 5′-cgtgacCTCGAGttaATATGTGGCCCTGTTCAG-3′, which corresponds to the 203 first N-terminal amino acids of Wcd (shown in Supplementary Information, Fig. S1a), thus excluding the WD40 motifs, with *Xho*I sites at both ends and a downstream stop codon. This PCR fragment was inserted at *Xho*I site in-frame into an N-terminal His-tag expression vector pET-16b (Novagen) and the DNA sequence was verified. Recombinant fusion protein expression was induced by IPTG in *Escherichia coli* strain BL21(DE3)pLysS (Invitrogen). The His–Wcd fusion protein was purified under native conditions using nickel-chelate-nitrilotriacetic acid (Ni-NTA) Superflow columns according to the supplier's instructions (Qiagen), followed by dialysis on Centricon YM-10 concentrators (Millipore). The final concentration of recombinant protein was achieved by SDS–PAGE on 12% gels and His–Wcd-containing polyacrylamide gel fragments were cut and used directly for immunization. A standard 3-month immunization protocol was performed by Eurogentec using two rabbits numbered 6011 and 6012. No further purification of the crude polyclonal antisera was needed, as both gave very little cross-immunoreactivity with other *Drosophila* epitopes. Both anti-Wcd antisera were used at a dilution of 1/5,000 for western blots and 1/500 for immunohistochemistry.

Live imaging. Ovaries were dissected in oil (10S, Halocarbon, Sigma). The muscular sheath around each ovariole was removed and germarium were made to stick to coverslips in oil. Germaria were imaged for 30–40 min with an Ultraview spinning disk (CSU10) operated by Metamorph on an inverted Leica DM IRBE microscope.

Larval NSCs. Third-stage larvae brains were obtained from larvae of the following genotype: w; *insc*-Gal4/+; UAS-*wcd*::GFP/+. Larval brains were dissected in dissection buffer (NaCl 136 mM, KCl 2.6 mM, NaH2PO4 0.36 mM, NaHCO3 12mM, glucose 5 mM in 100 ml water). The brains were dissociated in 0.2 mg ml^{-1} collagenase and washed in M3 medium. The neuroblasts were transfered to a chamber containing feeding buffer (Schneider's medium, 10% FCS, 5% fly extract, 1% penicillin/streptomycin, 1 mg ml^{-1} glucose, 5 $\mu g\ ml^{-1}$ insulin) and imaged. Images were acquired on an inversed LSM510 Zeiss confocal at 22 °C. SOP (pI cell) were imaged as described previously[48].

Co-immunoprecipitation. These experiments were performed with 50 µl of nProtein A Sepharose 4 Fast Flow (GE Healthcare) per experimental condition. Beads were first equilibrated by three 15-min washes in RIPA buffer (50 mM Tris-HCl pH 7.4, 2 mM EDTA, 100 mM NaCl, 0.5% IGEPAL CA-630 (Sigma), 10% glycerol, Complete EDTA-free protease inhibitor cocktail (Roche), phosphatase inhibitor cocktail set II (Calbiochem) and 200 units ml^{-1} RNasin RNase inhibitor (Promega)), and then incubated for 1 h at 4 °C in blocking buffer (RIPA buffer supplemented with 10% bovine serum albumin), followed by three more washes in RIPA buffer. Ovaries from 50 adult w^{1118} females per experimental condition were homogenized on ice and lysed for 30 min at 4°C in 300 µl of RIPA buffer. Homogenate was clarified by microfuge centrifugation for 15 min at 4 °C. The lysate was then cleared for 1 h at 4 °C with 50 µl of treated beads to eliminate non-specific direct interactions, and after centrifugation the supernatant was used as input for immunoprecipitation experiments. For Fib immunoprecipitation experiments, the ovarian extract was first incubated with 12 µl of anti-Fib antibody (ab5821, Abcam) overnight at 4 °C on a shaking table, before adding beads for another 4-h incubation. For Wcd immunoprecipitation experiments, beads were first incubated for 4 h at 4 °C on a shaking table with 20 µl of anti-Wcd antibody (or 20 µl of the corresponding pre-immune serum as a control), and then briefly washed once in RIPA buffer before adding the ovarian extract for an overnight incubation. In both Fib and Wcd immunoprecipitation experiments, a control with only beads and the ovarian extract (without any antibody) was included. Finally, beads were washed six times with 1 ml of RIPA buffer and then homogenized either in 50 µl of Laemmli buffer for protein extraction or in 1 ml of TRIzol reagent (Invitrogen) for RNA extraction. Each resulting protein or RNA extract was divided into two halves for loading on two gels of western or northern blot respectively.

Western blots. Denatured proteins were fractionated by SDS–PAGE using 10–12% gels and electroransferred to Protran nitrocellulose membranes (Schleicher & Schuell). The membranes were blocked overnight at 4 °C in blocking buffer (PBS buffer supplemented with 0.1% Tween 20 and 5% milk) and then incubated for 2 h in the same buffer containing primary antibodies at the following dilutions: anti-Wcd at 1/5,000 and anti-Fib (Abcam) at 1/500. After three washes in PBS-T

DOI: 10.1038/ncb1874

(PBS buffer supplemented with 0.1% Tween 20), membranes where incubated for 1 h with the secondary antibody in blocking buffer containing a peroxydase-conjugated light-chain-specific anti-rabbit IgG (Jackson Immunoresearch) diluted at 1/10,000. After three washes in PBS-T, bands were detected with the SuperSignal West Pico Chemiluminescent Substrate (Pierce) and visualized using a LAS-3000 Imaging System (Fujifilm).

Northern blots. Total RNAs from wild-type or RNAi-treated S2 cells, co-immunoprecipitation samples or polysome gradient fractions were prepared with TRIzol reagent following the supplier's instructions (Invitrogen). Glycogen (35 μg; MP Biomedicals) was added as a carrier for RNA precipitation of all co-immunoprecipitation samples and polysome gradient fractions. Denatured RNA samples were run overnight on either 1% (in the case of high molecular weight pre-rRNAs) or 2% (in the case of the U3 snoRNA) agarose formadehyde gels in sodium phosphate buffer and were then transferred in 20 × SSC to Hybond N^+ membranes (GE Healthcare). After methylene blue staining, membranes were pre-hybridized for 4 h in 3 × SSC, 0.2% (w/vol) polyvinylpyrrolidone 40, 0.2% (w/vol) Ficoll 400, 1% (w/vol) glycine, 5% (w/vol) polyethylene glycol 6000, 1% (w/vol) SDS and 100 μg $ml^{-1}$of denatured DNA from salmon sperm, before an overnight hybridization under the same conditions. Oligonucleotide probes were labelled at their 5′ ends with g-^{32}P-ATP (GE Healthcare) using T4 polynucleotide kinase (New England Biolabs). DNA fragments used as probes were labelled by random priming with a-^{32}P-dCTP (GE Healthcare) using the Megaprime DNA labelling system (GE Healthcare). All probes were purified on Probe Quant G50 micro-columns (GE Healthcare). Pre-hybridization, hybridization and washing steps were carried out at 42 °C for oligonucleotide probes and at 65 °C for DNA fragment probes. Membranes were subjected to phosphoimager analysis using a Typhoon Trio Imaging System (GE Healthcare). Oligonucleotide probes, corresponding to different regions of the pre-rRNA precursor, are shown in Fig. 3d and have the following sequences: ITS1.2 is 5′-GATTTTAACTTTTGATTCCATGGAATC-3′, ITS1.3 is 5′-GAAATTAAAAATACACCATTTTACTGGC-3′, ITS1.4 is 5′-GTCAATTATGTTTTTATTGAAAGAAATTAAAAATAC-3′, ITS2 is 5′-GAATCATTAATAAGAGACAATTCTAGATG-3′ and 28S is 5′-GTTACAAAAGTCGTTTACAATTGATTC-3′. The pre-rRNA precursor was also detected with a DNA probe corresponding to the ITS1 region, obtained by PCR amplification from w^{1118} genomic DNA using primers 5′-GTATGTTGTGCGTATTTGTG-3′ and 5′-TAATCTGGTTGGTTATGGGG-3′. Detection of the U3 snoRNA was performed using as probe a PCR fragment amplified from w^{1118} genomic DNA using primers 5′-CTTTCACACTAGCTGAAAGCCAAGT-3′ and 5′-ACCACTCAGAATTCGCTCTATCCG-3′.

Cell culture and RNA interference. *Drosophila* S2 cells were grown in Schneider's *Drosophila* medium (Invitrogen) supplemented with 10% heat-inactivated fetal bovine serum (Biowest), 100 units ml^{-1} penicillin and 100 μg ml^{-1} streptomycin (Sigma) at 25 °C. RNA interference was performed as described previously[49] with little modification. A PCR fragment containing 5′ T7 RNA polymerase-binding sites and corresponding to *wcd* 465 first nucleotides was amplified from plasmid DNA (DGRC cDNA clone no. LD16320), using primers 5′-gaattgtaatacgactcactatagggATGAGTTCAGACGAGTCCA-3′ and 5′-gaattgtaatacgactcactatagggGACCTTCTTTTCCGCCCACT-3′. This DNA template was transcribed using the Megascript RNAi kit following the supplier's instructions (Ambion). S2 cells were seeded in 25- or 75-cm^2 flasks at a density of 10^6 cells ml^{-1} and 10^5 cells/cm^2, and treated with *wcd* RNAi (25 μg per 10^6 cells) for 1 h in 1 ml of serum-free Schneider's medium per 10^6 cells, followed by 4 days in a total of 3 ml of complete Schneider's medium per 10^6 cells. The efficiency of *wcd* RNAi-mediated depletion was assessed by western blot.

Immunostaining and *in situ* hybridization. For immunostaining, ovaries were dissected in PBS, fixed in 4%PFA-PEPS, permeabilized in PBT (0,2%Triton) for 30 min, washed 2 h in PBS, left overnight with primary antibodies in PBS at room temperature, washed 2 h in PBS, left with secondary antibody for 2hr at room temperature, washed 1 h in PBS and mounted in Cityfluor. We used the following primary antibodies: rabbit anti-Wcd at 1/500; mouse anti-Orb (orb4H8 and orb6H4 DHSB) 1/250; rabbit anti-C(3)G at 1/1,000 (ref. 50); anti-H3K27me3; anti-H3K9me2; anti-activated caspase3 (AbCam); human anti-Fib at 1/500 (gift from D. Hernandez-Verdun, Institut Jacques Monod, France); rabbit anti-Fib at 1/500 (AbCam); rabbit anti-LSM11 at 1/1000 (ref. 25); rabbit anti-phosphohistoneH3 (Upstate) 1/1,000; mouse anti-α-Spectrin (3A9, DHSB), rabbit anti-Chinmo 1/1,000 (ref. 51), rabbit anti-Br-C 1/500, and rabbit anti-Miranda[52]. Secondary antibodies conjugated with Cy3, Cy5 and TRITC (Jackson laboratories) were used at 1/200. Samples were examined either with a Leica DMR microscope or by confocal microscopy using a Leica SP5 AOBS microscope. *In-situ* hybridizations were performed as published previously[53]

47. Bellaiche, Y., Gho, M., Kaltschmidt, J. A., Brand, A. H. & Schweisguth, F. Frizzled regulates localization of cell-fate determinants and mitotic spindle rotation during asymmetric cell division. *Nature Cell Biol.* **3,** 50–57 (2001).
48. Gho, M., Bellaiche, Y. & Schweisguth, F. Revisiting the Drosophila microchaete lineage: a novel intrinsically asymmetric cell division generates a glial cell. *Development* **126,** 3573–3584 (1999).
49. Worby, C. A., Simonson-Leff, N. & Dixon, J. E. RNA interference of gene expression (RNAi) in cultured *Drosophila* cells. *Sci. STKE* 2001, PL1 (2001).
50. Hong, A., Lee-Kong, S., Iida, T., Sugimura, I. & Lilly, M. A. The p27cip/kip ortholog dacapo maintains the *Drosophila* oocyte in prophase of meiosis I. *Development* **130,** 1235–1242 (2003).
51. Zhu, S. *et al.* Gradients of the *Drosophila* Chinmo BTB-zinc finger protein govern neuronal temporal identity. *Cell* **127,** 409–422 (2006).
52. Ikeshima-Kataoka, H., Skeath, J. B., Nabeshima, Y.-i., Doe, C. Q. & Matsuzaki, F. Miranda directs Prospero to a daughter cell during *Drosophila* asymmetric divisions. *Nature* **390,** 625–629 (1998).
53. González-Reyes, A., Elliott, H. & St Johnston, D. Polarization of both major body axes in *Drosophila* by *gurken-torpedo* signalling. *Nature* **375**, 654–658 (1995).

nature cell biology

DOI: 10.1038/ncb1874

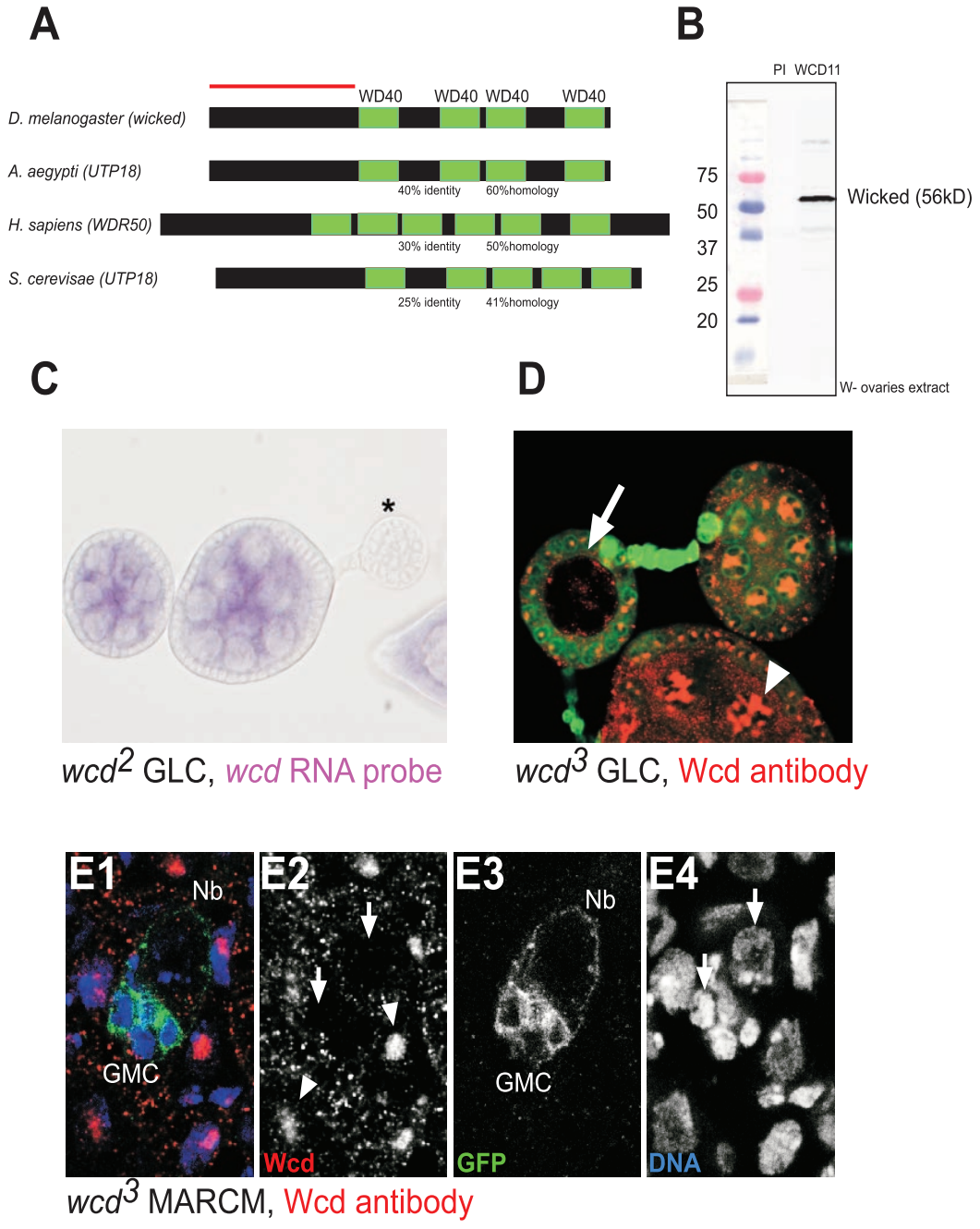

Figure S1 Wcd homologues and specificity of the antibody. **(A)** Wcd homologues. The WD40 domains are in green. In red the region used to make the antibody. **(B)** Western blot using the Wcd antibody on ovarian extracts. One major band at the expected size is detected. **(C)** *In situ* hybridization with a *wcd* RNA probe on *wcd* mutant germline clone. No signal is detected in the homozygous mutant egg chamber (asterisk). **(D)** Immunostaining using the Wcd antibody on a wcd^3 mutant germline clone. Wcd is in red and the clone is labelled by the lack of nuclear GFP (in green). No signal is detected in the homozygous mutant egg chamber (arrow) and Wcd is nucleolar in WT cells (arrowhead pointing at a WT nurse cell nucleus). **(E)** wcd^3 MARCM clone in the larval ventral nerve cord. **(E1)** The endogenous Wcd protein is in red, the DAPI staining in blue labels DNA and mutant cells are labelled by the presence of membrane associated GFP. Single channels are shown in **(E2-E4)**. No Wcd protein is detected in wcd^3 mutant NBs or GCs (arrows). WT NBs show strong nucleolar Wcd staining (arrowheads in **E2**).

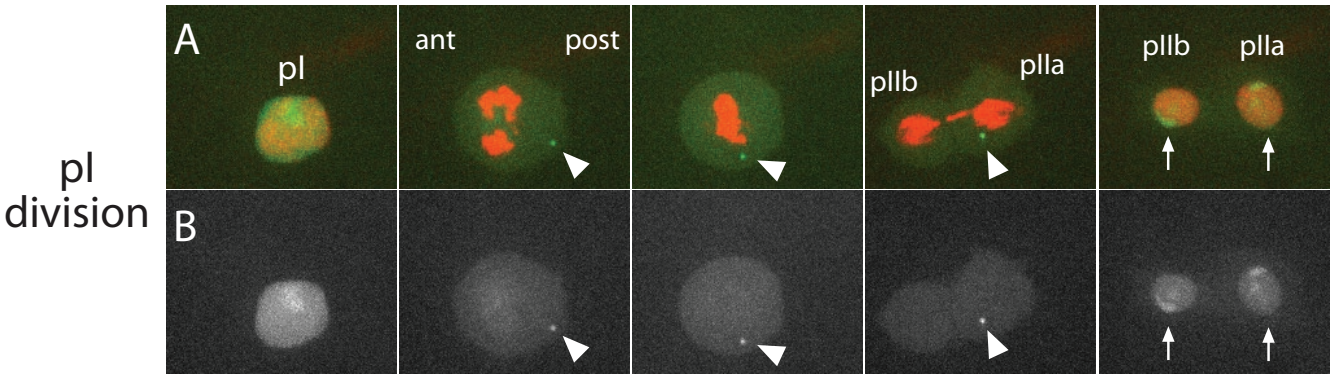

Figure S2 Asymmetric segregation of Wcd during pI division in the peripheral nervous system. Wcd::GFP is in green. H2B::RFP is in red. **(A)** Wcd::GFP forms a dot when the nuclear envelop breaks down (arrowhead) upon pI division. The dot is located on the side of the future pIIa cell. At the end of telophase, both nucleoli reform (arrow). Single channel is shown in **(B)** Wcd::GFP.

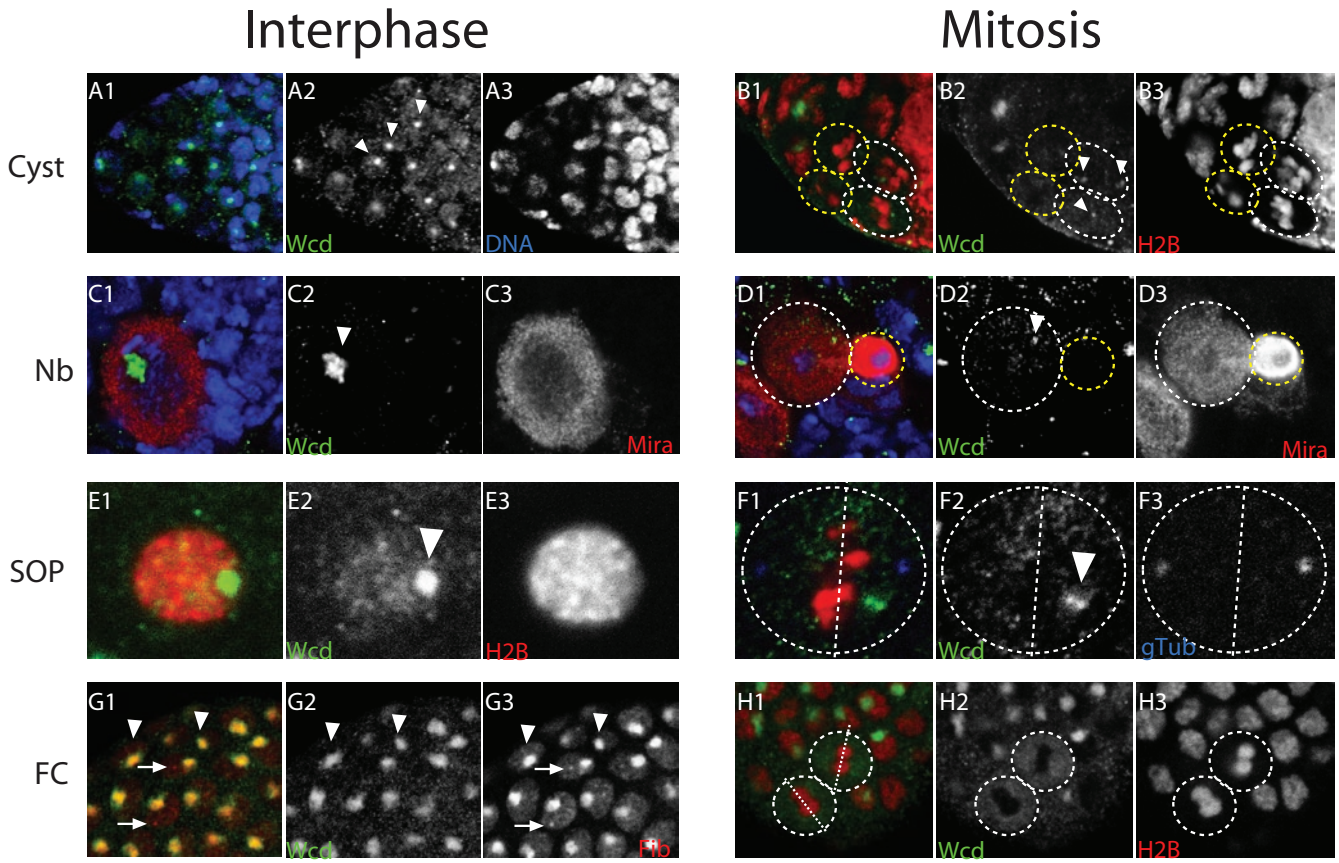

Figure S3 Localisation of the endogenous Wcd protein in cyst cells, neuroblasts, sensory organ precursors and follicle cells during interphase and mitosis. **(A1, B1, C1, D1, E1, F1, G1, H1)** The endogenous Wcd protein is in green. **(A, C, E, G)** Cells in interphase. **(B, D, F, H)** Mitotic cells. **(A,B)** Cyst cells. **(C, D)** NBs. **(E,F)** Sensory organ precursor cells (SOPs). **(G,H)** Follicle cells (FC). **(A)** Wcd is nucleolar in cyst cells during interphase (arrowheads in **A2**). The DAPI staining is in blue in **(A1)**. Single channels are shown in **(A2, A3)**. **(B)** Particles of Wcd are asymmetrically segregated upon cyst cell division (arrowheads in **B2**) into the two pro-oocytes (highlighted by white dashed circles). The yellow dashed circles highlights the two nurse cells. The H2B::RFP fusion protein is shown in red in **(B1)**. Single channels are shown in **(B2, B3)**. **(C)** Wcd is nucleolar in NBs during interphase (arrowhead in **C2**). **(C1)** Mira is in red and the DAPI staining is in blue. Single channels are shown in **(C2, C3)**. **(D)** Particules of Wcd are asymmetrically segregated upon NB division (arrowhead in **D2**) into the NB (highlighted by a white dashed circle). The yellow dashed circle highlights the future ganglion mother cell. **(D1)** Mira is in red and the DAPI staining is in blue. Single channel are shown in **(D2, D3)**. **(E)** Wcd is nucleolar in SOPs during interphase (arrowhead in **E2**). **(E1)** H2B::RFP is in red. Single channels are shown in **(E2, E3)**. **(F)** Particles of Wcd that do not co-localise with centrosomes are asymmetrically segregated upon SOP division (arrowhead in **F2**). The white dashed circle highlights the dividing SOP and the orientation of the metaphase plate is indicated by a white straight dashed line. **(F1)** H2B::RFP is in red and the centrosome marker γ-tubulin is in blue. Single channel are shown in **(F2, F3)**. **(G)** Wcd co-localises with Fibrillarin in the nucleolus of the follicle cells (arrowheads) but only Fibrillarin is detected in the Cajal Body (arrows). **(G1)** Fibrillarin is in red. Single channels are shown in **(G2, G3)**. **(H)** Wcd is symmetrically distributed upon follicle cell division. The white dashed circles highlight dividing follicle cells and the orientation of the metaphase plate is indicated by a white straight dashed line. H2B::RFP is in red in **(H1)** and single channels are shown in **(H2, H3)**.

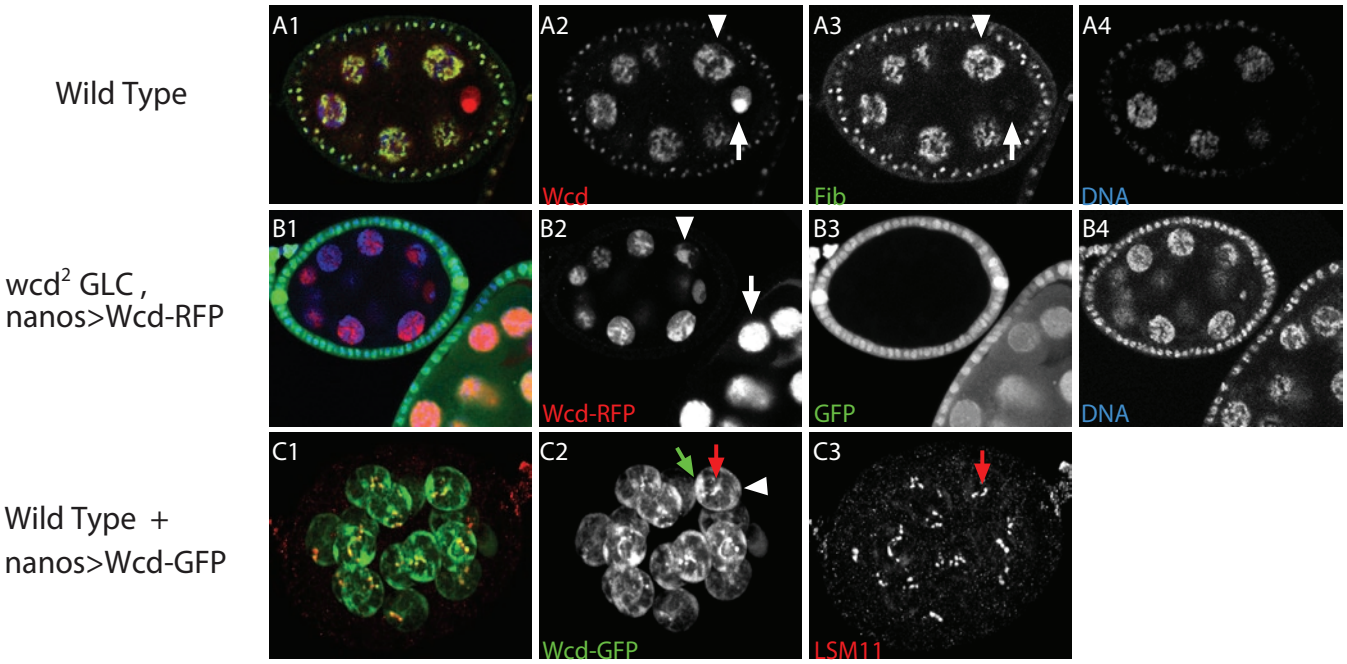

Figure S4 (Fichelson et al.)

Figure S4 Comparison of the localisation of the endogenous Wicked protein with RFP- or GFP-tagged Wicked in stage 5 egg chambers. **(A)** The endogenous Wcd protein perfectly colocalises with Fibrillarin in the nucleolus of the nurse cells (arrowhead) but is present without Fibrillarin in the gernminal vesicle (arrow). **(A1)** Wcd is in red, Fibrillarin in green and the DAPI staining is in blue. Single channels are shown in **(A2-A4)**. **(B)** RFP::Wcd localisation in the absence of the endogenous Wcd protein (rescue experiment). Cells lacking endogenous Wcd are labelled by the lack of nuclear GFP. **(B1)** RFP::Wcd is in red, GFP is in green and the DAPI staining is in blue. Single channels are shown in **(B2-B4)**. In the context of a rescue, RFP::Wcd is nucleolar, similarly to the endogenous Wcd (arrowhead in **B2**). When RFP::Wcd is expressed in the presence of the endogenous Wcd protein, the fusion protein fills most of the nucleus (arrow in **B2**). **(C)** Mild over-expression of Wcd::GFP in the presence of the endogenous Wcd protein. **(C1)** Wcd::GFP is in green and the histone locus body marker LSM11 is in red. Single channels are shown in **(C2, C3)**. Although the endogenous protein is present, Wcd::GFP accumulates in descrete regions of the nucleus: in the nucleolus (green arrow in **C2**) and in the histone locus body (red arrow in **C2, C3**). The rest of the nucleoplasm shows only low levels of Wcd::GFP (white arrowhead in **C2**).

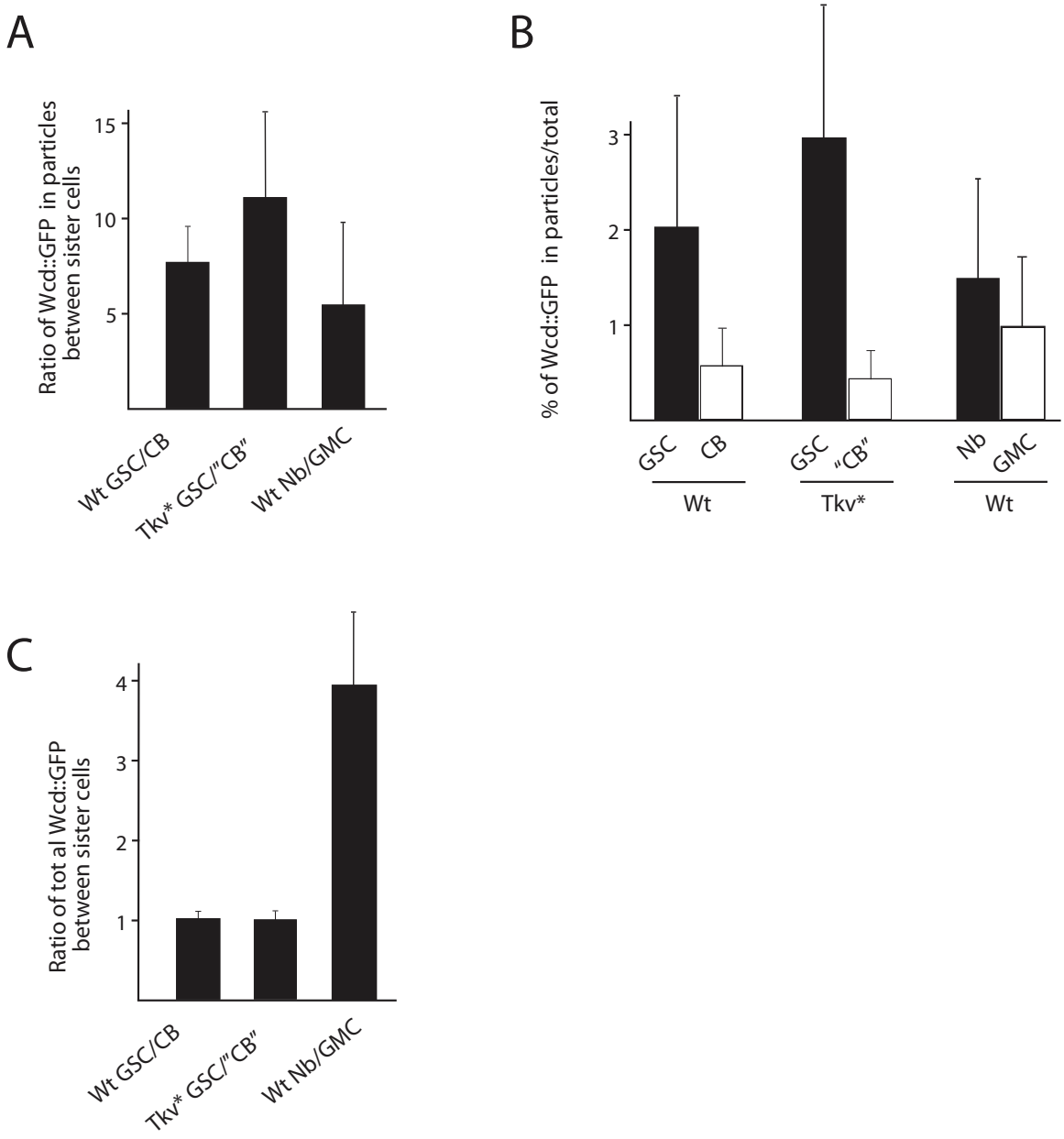

Figure S5 Quantification of the asymmetric distribution of the Wcd particles in different cell types upon mitosis. **(A)** Ratio of Wcd::GFP in particles between sister cells during the division of WT GSCs, GSCs expressing the activated form of thick veins (tkv*-GSC) and WT NBs. CB: cystoblast. GMC: ganglion mother cell. **(B)** Percentage of Wcd::GFP present in particles in WT GSCs and WT CBs; tkv*-GSC and "CB"; NBs and GMCs. **(C)** Ratio of total Wcd::GFP between sister cells upon WT GSCs division, tkv*-GSC division and NB division.

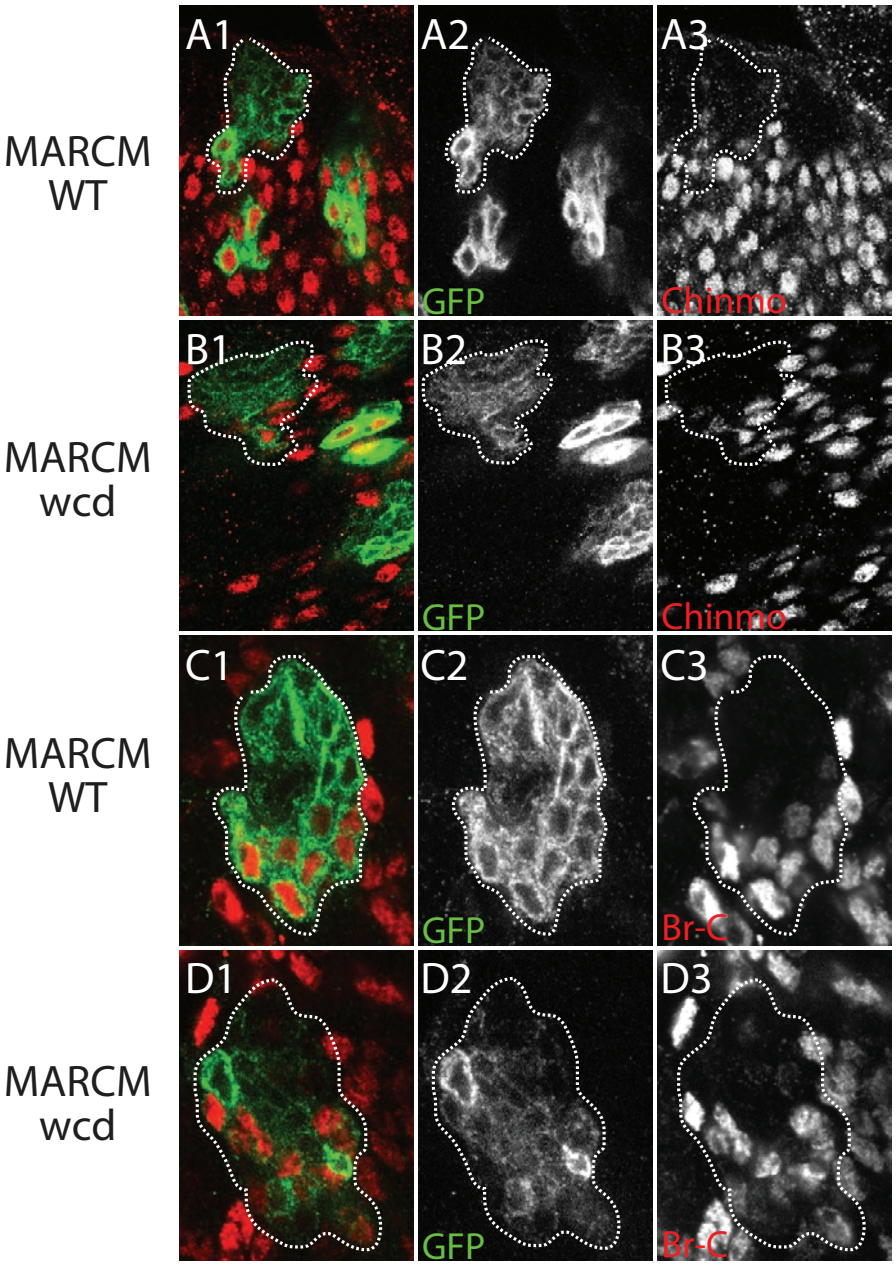

Figure S6 *wcd* mutant neuroblasts produce cells expressing the correct postmitotic transcription factors. **(A, C)** WT MARCM clone. **(B, D)** *wcd*^{3} MARCM clone. **(A-D)** The clone is labelled by the presence of a membrane associated GFP and highlighted by a white dashed line. **(A1, B1, C1, D1)** GFP is in green. **(A,B)** A subset of the clone expresses Chinmo (in red in A1 and B1), whether in the presence **(A)** or in the absence of Wcd **(B)**. Single channels are shown in **(A2, A3, B2, B3)**. **(C-D)** A subset of the clone expresses Broad-Complex (Br-C, in red in **C1** and **D1**), whether in the presence **(C)** or in the absence of Wcd **(D)**. Single channels are shown in **(C2, C3, D2, D3)**.

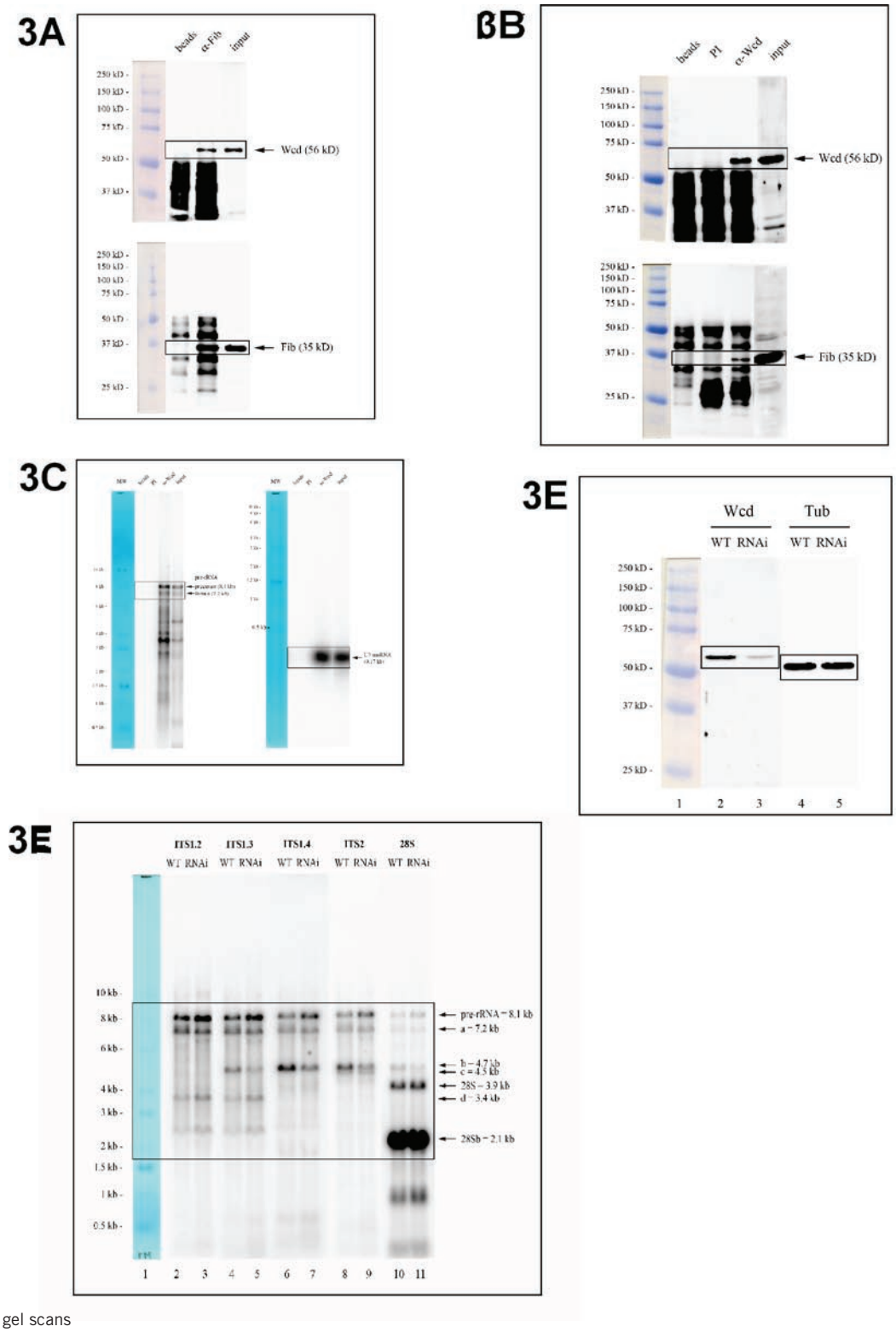

Figure S7 Full gel scans

Supplementary Movie Legends

Movie 1 Wcd segregates asymmetrically into the germline stem cell (anaphase). Wcd::GFP is in green and HistoneH2B::RFP (H2B::RFP) is in red. Arrowhead: large dot of Wcd::GFP segregating into the germline stem cell (GSC). Note that some Wcd::GFP also segregates into the cystoblast (CB).

Movie 2 Wcd segregates asymmetrically into the germline stem cell (metaphase). Wcd::GFP is in green and H2B::RFP is in red. One dot of Wcd::GFP (arrowhead) forms at nuclear envelop break down (NEB) and localizes at the anterior side of the metaphase plate toward the GSC.

Movie 3 Wcd segregates asymmetrically into the pro-oocytes. Wcd::GFP is in green and H2B::RFP is in red. Synchronous division of a 2-cell cyst to form a 4-cell cyst. Large aggregates of Wcd::GFP localize into the two pro-oocytes (arrowheads). Note that the two future nurse cells also inherit some Wcd::GFP (arrows).

Movie 4 Wcd segregates asymmetrically into the pro-oocytes. Wcd::GFP is in green and H2B::RFP is in red. Synchronous division of a 2-cell cyst to form a 4-cell cyst. One dot of Wcd::GFP forms after NEB in each cell (only one is first shown then both with an arrowhead) and segregate into the two inner cells (white circles, pro-oocytes). Yellow circles: pro-nurse cells.

Movie 5 Wcd segregates asymmetrically in germline cells expressing an activated form of thickvein. Wcd::GFP is in white. Overexpression of Tkv under the control of the *nanos*-GAL4 driver. Two dots of Wcd::GFP (arrowheads) segregate into only one cell.

Movie 6 Wcd segregates asymmetrically in germline cells expressing an activated form of thickvein. Wcd::GFP is in white. Overexpression of Tkv under the control of the *nanos*-GAL4 driver. Two independent GSC-like cells dividing away from the niche. Wcd::GFP forms aggregates (arrowhead) at nuclear envelop break down (NEB). Wcd::GFP (arrowheads) segregates into only one cell in both cases.

Movie 7 Wcd segregates asymmetrically during larval neuroblast division. Wcd::GFP is in white. One neuroblast (NB) is shown with part of its progeny (GMC). Two dots of Wcd::GFP (arrowheads) segregate into the neuroblast (white circle) at anaphase and fuse with the nucleolus at interphase.

Movie 8 Wcd segregates asymmetrically during larval neuroblast division. Wcd::GFP is in white. One neuroblast (NB) is shown with part of its progeny (GMC). Two dots of Wcd::GFP (arrowheads) segregate into the neuroblast (white circle) at anaphase and fuse with the nucleolus at interphase.

Movie 9 Wcd segregates asymmetrically into the pIIa cell during Sensory Organ Precursor division (SOP). Wcd::GFP is in green and H2B::RFP is in red. Two SOP divisions are shown. One dot of Wcd::GFP (arrowhead) forms at nuclear envelop breakdown (NEB) and segregates into the posterior pIIa cell in both cases.

Movie 10 Wcd segregates symmetrically during follicle cell divisions. Wcd::GFP is in white. Armadillo::GFP is also in white and labels the adherens junctions at the cortex of follicle cells (only a few junctions are visible in this movie). 3 follicle cells divisions are shown. No particle form after nuclear envelop breakdown (NEB) and cytoplasmic Wcd::GFP is partitioned equally between sister cells.